J. Am. Chem. Soc. **1995,** *117,* 2259−2272

Ligand K-Edge X-ray Absorption Spectroscopic Studies: Metal−Ligand Covalency in a Series of Transition Metal Tetrachlorides

Susan E. Shadle,[†] Britt Hedman,*,[‡] Keith O. Hodgson,*,[†,‡] and Edward I. Solomon*,[†]

Contribution from the Department of Chemistry and Stanford Synchrotron Radiation Laboratory, Stanford University, Stanford, California 94305

Received August 4, 1994[⊗]

Abstract: X-ray absorption spectra (XAS) have been measured at the chlorine K-edge for a series of tetrahedral MCl_4^{n-} complexes ($M = Cu^{II}$, Ni^{II}, Co^{II}, Fe^{II}, and Fe^{III}) to investigate ligand−metal bonding. The intensity of the pre-edge feature in these spectra reflects excited-state multiplet effects, intermediate-strength ligand field excited-state mixing, and ligand−metal covalency in the partially occupied d-orbital-derived molecular orbitals of each complex. A methodology which relates covalency to pre-edge intensity for d^{10-n} hole systems ($n \geq 1$) is developed. Application of this methodology to the experimental data provides quantitative information about the covalency of the ligand−metal bond. The energy of the pre-edge feature is related to both the charge on the ligand and the metal d-derived orbital energy. An analysis of the pre-edge and edge energies allows the relative energy of the metal d-manifold, as well as the charge on each chloride ligand, to be quantitated. Results show that the HOMO covalency decreases across the series from $Cu^{II}Cl_4^{2-}$ to $Fe^{II}Cl_4^{2-}$, while that of $Fe^{III}Cl_4^{-}$ is larger than that of $Fe^{II}Cl_4^{2-}$. This is related to the experimentally determined d-manifold energies, which vary in the order $Fe^{III} < Cu^{II} < Ni^{II} < Co^{II} < Fe^{II}$. The metal centers with the deepest d-manifold energies (closest to the ligand 3p orbital energy) are involved in the strongest ligand−metal bonding interactions and exhibit the largest metal d-derived orbital covalency. The total charge donated by the chloride ligands to the metal is greatest in $Fe^{III}Cl_4^{-}$, and the variation observed is similar to that seen for the metal d-derived orbital covalency: $Fe^{III} > Cu^{II} > Fe^{II} \sim Co^{II} \sim Ni^{II}$. This study extends ligand K-edge XAS to the investigation of ligand−metal bonding in d^{10-n} hole systems ($n \geq 1$) and forms the foundation for future ligand K-edge XAS studies of electronic structure in transition metal centers.

Introduction

Analysis of X-ray absorption edge spectra can provide insight into the electronic structure of an absorbing atom.[1,2] While this technique has been used extensively at the K-edge of transition metal centers such as Cu, Fe, Ni, and Mo,[3−6] it has also recently been demonstrated that the absorption edges of ligands such as S and Cl can be used to study the electronic structure of inorganic Cu^{II} complexes[7−9] and cupric protein active sites.[8] The 3p orbitals of S and Cl ligands are directly involved in bonding with transition metal ions. Because the electric dipole-allowed transitions for K-edges are 1s → *n*p, ligand K-edge X-ray absorption spectroscopy provides a direct probe of these ligand−metal bonding interactions.

The K-edge absorption of a ligand, such as chloride, bound to a d^9 copper ion exhibits a well-defined pre-edge feature which is assigned as a ligand 1s → ψ^* transition, where ψ^* is the half-filled, highest-occupied molecular orbital (HOMO) in Cu^{II}. Due to the localized nature of the Cl 1s orbital, this transition can have absorption intensity only if the half-filled HOMO orbital contains a significant component of Cl 3p character as a result of covalency. A more complete description of this Cl 1s → ψ^* transition involves $\psi^* = (1 - \alpha'^2)^{1/2}[\text{Cu 3d}] - \alpha'[\text{Cl 3p}]$, where α'^2 represents the amount of Cl 3p character in the HOMO. The observed pre-edge transition intensity is simply the intensity of the pure dipole-allowed Cl 1s → 3p transition weighted by α'^2 (eq 1)

$$I(\text{Cl 1s} \rightarrow \psi^*) = \alpha'^2 I(\text{Cl 1s} \rightarrow \text{Cl 3p}) \tag{1}$$

Thus, the pre-edge intensity provides a *direct* probe of the ligand contribution to the HOMO due to bonding. Ligand K-edge XAS provides information similar to that obtained from analysis of ligand superhyperfine splittings in EPR spectroscopy. However, unlike ligand superhyperfine analysis, ligand K-edge XAS is not limited to the investigation of ligands with a nuclear spin or complexes with an EPR signal.

The relationship between intensity and covalency described above (eq 1) for ligand−Cu^{II} interactions is straightforward because Cu^{II} is d^9 and thus has a single half-occupied HOMO (ψ^*). Here the technique of ligand K-edge XAS is

---

* Persons to whom correspondence should be addressed.

[†] Stanford University, Department of Chemistry.

[‡] Stanford Synchrotron Radiation Laboratory.

[⊗] Abstract published in *Advance ACS Abstracts,* February 1, 1995.

(1) Heald, S. M.; Tranquada, J. M. In *Physical Methods of Chemistry*; Rossiter, B. W., Hamilton, J. F., Eds.; Wiley: New York, 1990; Vol. 5, pp 189−272.

(2) Bianconi, A. In *X-ray Absorption*; Koningsberger, D. C., Prins, R., Eds.; Wiley: New York, 1988; pp 573−662.

(3) Kau, L. S.; Spira-Solomon, D. J.; Penner-Hahn, J. E.; Hodgson, K. O.; Solomon, E. I. *J. Am. Chem. Soc.* **1987**, *109*, 6433−6442.

(4) Roe, A. L.; Schneider, D. J.; Mayer, R. J.; Pyrz, J. W.; Widom, J.; Que, L., Jr. *J. Am. Chem. Soc.* **1984**, *106*, 1676−1681.

(5) Eidsness, M. K.; Sullivan, R. J.; Scott, R. A. In *Bioinorganic Chemistry of Nickel*; Lancanster, J. R., Ed.; VCH: Deerfield Beach, FL, 1988; pp 73−92.

(6) Conradson, S. D.; Burgess, B. K.; Newton, W. E.; McDonald, J. W.; Rubinson, J. R.; Gheller, S. F.; Mortenson, L. E.; Adams, M. W. W.; Mascharack, P. K.; Armstrong, W. A.; Holm, R. H.; Hodgson, K. O. *J. Am. Chem. Soc.* **1985**, *107*, 7935−7940.

(7) Hedman, B.; Hodgson, K. O.; Solomon, E. I. *J. Am. Chem. Soc.* **1990**, *112*, 1643−1645.

(8) Shadle, S. E.; Penner-Hahn, J. E.; Schugar, H. J.; Hedman, B.; Hodgson, K. O.; Solomon, E. I. *J. Am. Chem. Soc.* **1993**, *115*, 767−776.

(9) Shadle, S. E.; Hedman, B.; Hodgson, K. O.; Solomon, E. I. *Inorg. Chem.* **1994**, *33*, 4235−4244.

0002-7863/95/1517-2259$09.00/0

Table 1. Structural Parameters for $\sim T_d$ MCl_4^{n-} Complexes

MCl_4^{n-} Complex[a]	average bond length (Å)	angles (deg)	related complex	average bond length (Å)	angles (deg)
Cs_2CuCl_4[b]	2.230	100−131			
$(Ph_3MeAs)_2NiCl_4$[c]	2.269	109.1−109.4	$(Et_4N)_2NiCl_4$[d]	2.245	107−111
			$(Me_4N)_2NiCl_4$[e]	2.234	108−111
$(Ph_3MeAs)_2CoCl_4$[c]	isomorphous w/nickel complex		$(Me_4N)_2CoCl_4$[e]	2.254	108−111
$(Et_4N)_2FeCl_4$			$(Me_4N)_2FeCl_4$[f]	2.293	108−114
$(Et_4N)FeCl_4$			$(Ph_4As)FeCl_4$[g]	2.182	106−115

[a] Complexes for which Cl K-edge data were measured. [b] Reference 11. [c] Reference 23. [d] Stucky, G. D.; Folkers, J. B.; Kistenmacher, T. J. *Acta Crystallogr.* **1967**, *23*, 1064−1070. [e] Wiesner, J. R.; Srivastava, R. C.; Kennard, C. H. L.; DiViara, M.; Lingafelter, E. C. *Acta Crystallogr.* **1967**, *23*, 565−574. [f] Reference 25. [g] Reference 26.

extended to other metal ions. As in Cu^{II} systems, the pre-edge feature in other d^n metal centers corresponds to a transition (or several transitions) from a ligand 1s orbital to unoccupied or partially-occupied antibonding orbitals with both metal d- and ligand p-character. However, in systems with more than one d-manifold electron or hole, several many-electron excited states are possible, and transitions to more than one partially-occupied metal d-derived orbital are possible. Further, multiplet effects in the d^{n+1} excited state can affect the observed intensity. The analysis of pre-edge intensity for the determination of covalency in metal d-derived orbitals requires that all contributions to the intensity be taken into account.

This study examines the Cl K-edge XAS pre-edge features for the tetrahedral metal−tetrachloride series MCl_4^{n-}, where M = Cu^{II}, Ni^{II}, Co^{II}, Fe^{II}, and Fe^{III}. The antibonding metal d-derived orbitals in T_d metal complexes are a t_2- and an e-set. The t_2-set has both Cl $3p_\sigma$ and Cl $3p_\pi$ interactions, while the e-set has only Cl $3p_\pi$-character. In T_d Cu^{II},[10] there is a single vacancy in the t_2-set, while Ni^{II} and Co^{II} are characterized by two and three t_2 holes, respectively. The T_d Fe^{II} center has three t_2 holes and a single hole in the e-set. In the T_d Fe^{III} complex, each of the d-type orbitals is half-occupied, with three t_2 holes and two e holes. Thus, in T_d Cu^{II}, Ni^{II}, and Co^{II}, pre-edge transitions will correspond only to transitions to the t_2-set of antibonding orbitals, while in Fe^{II} and Fe^{III} transitions to the e-set are also possible.

A methodology for interpreting pre-edge intensities and energies is developed for these d^n hole systems ($n \geq 1$). The contribution to pre-edge intensity from multiplet effects is determined, and expressions which relate experimental intensity to covalency are derived. The effect on pre-edge intensity from the mixing of excited states in ligand fields of intermediate strength is defined, and the ligand−metal covalency of each T_d site is quantitatively determined from the experimental pre-edge intensity. The experimental estimates of covalency are compared to SCF-Xα-SW (Xα) calculations on each complex. Finally, analysis of the pre-edge and edge energies provides quantitative information[9] about variation in chloride charge donation as well as relative shifts in the d-manifold energy of each metal center. These results are correlated with the experimentally determined covalency in each complex.

Experimental Section

A. Samples and Sample Preparation. A summary of the structural parameters for each of the complexes included in this study is provided in Table 1. Cs_2CuCl_4 was prepared according to published methods.[11,12] The remaining compounds, $(Ph_3MeAs)_2NiCl_4$, $(Ph_3MeAs)_2CoCl_4$, $(Et_4N)_2FeCl_4$, and $(Et_4N)FeCl_4$, were prepared as described in the literature.[13] The $(Et_4N)_2FeCl_4$ sample was prepared under anaerobic conditions.

For the X-ray absorption experiments, samples were ground into a fine powder (at least several minutes of grinding with mortar and pestle). The powder was dispersed as thinly as possible (to minimize the possibility of self-absorption) on Mylar tape. The procedure has been verified to minimize self-absorption effects in the data by systematically testing samples with progressively less absorption (less coverage and smaller particle size) until the observed intensity no longer varies with the thickness of the sample. The Mylar tape contained an acrylic adhesive which was determined to have a level of chlorine contaminants below that which is detectable under the conditions of the X-ray absorption measurements. The powder on tape was mounted across the window of an aluminum plate. The $(Et_4N)_2FeCl_4$ sample was prepared in a dry, anaerobic atmosphere. A 6.35 μm polypropylene film window protected the sample from exposure to air.

B. X-ray Absorption Measurements. X-ray absorption data were measured at the Stanford Synchrotron Radiation Laboratory using the 54-pole wiggler beamline 6-2 in low magnetic field mode (5 kG) with a Pt-coated focusing mirror and a Si(111) double crystal monochromator, under dedicated conditions (3.0 GeV, ~50 mA). The monochromator was detuned ~30% to eliminate higher harmonic components in the X-ray beam. Details of the optimization of this set-up for low energy studies have been described in an earlier publication.[14]

All Cl K-edge measurements were made at room temperature. The data were collected as fluorescence excitation spectra utilizing an ionization chamber as a fluorescence detector.[15,16] Several (two to three) scans were measured for each sample. The energy was calibrated from the Cl K-edge spectra of Cs_2CuCl_4, run at intervals between the samples. The maximum of the first edge-region feature in the spectrum was assigned to 2820.20 eV. Scans ranged from 2740 to 3100 eV, with a step size of 0.08 eV in the edge region. The spectrometer energy resolution was ~0.5 eV.[14] Calculating and comparing first and second derivatives for model compounds measured repeatedly during different experimental sessions results in a reproducibility in edge position of ~0.1 eV for these experiments.

C. Data Reduction. Data were averaged and a smooth background was removed from all spectra by fitting a polynomial to the pre-edge region and subtracting this polynomial from the entire spectrum. Normalization of the data was accomplished by fitting a flat polynomial or straight line to the post-edge region and normalizing the edge jump to 1.0 at 2840 eV.

D. Fitting Procedures. The intensities of pre-edge features were quantitated by fits to the data. The fitting program EDG_FIT, which utilizes the double precision version of the public domain MINPAK fitting library[17] was used. EDG_FIT was written by Dr. Graham N. George of the Stanford Synchrotron Radiation Laboratory. Pre-edge features were modeled by pseudo-Voigt line shapes (simple sums of Lorentzian and Gaussian functions). This line shape is appropriate as the experimental features are expected to be a convolution of the Lorentzian transition envelope[18] and the Gaussian lineshape imposed

---

(10) The geometry of the $CuCl_4^{2-}$ complex in this study is D_{2d}. This geometric distortion from T_d will be addressed as necessary throughout the text.

(11) McGinnety, J. A. *J. Am. Chem. Soc.* **1972**, *94*, 8406−8412.

(12) Sharnoff, M. *J. Chem. Phys.* **1965**, *42*, 3383−3395.

(13) Gill, N. S.; Taylor, F. B. *Inorg. Synth.* **1967**, *9*, 136−142.

(14) Hedman, B.; Frank, P.; Gheller, S. F.; Roe, A. L.; Newton, W. E.; Hodgson, K. O. *J. Am. Chem. Soc.* **1988**, *110*, 3798−3805.

(15) Lytle, F. W.; Greegor, R. B.; Sandstrom, D. R.; Marques, E. C.; Wong, J.; Spiro, C. L.; Huffman, G. P.; Huggins, F. E. *Nucl. Instrum. Methods* **1984**, *226*, 542−548.

(16) Stern, E. A.; Heald, S. M. *Rev. Sci. Instrum.* **1979**, *50*, 1579−1582.

(17) Argonne National Laboratory; Garbow, B. S.; Hillstrom, K. E.; More, J. J.

(18) Agarwal, B. K. *X-ray Spectroscopy*; Springer-Verlag: Berlin, 1979; pp 276 ff.

by the spectrometer optics.[15,19,20] A fixed 1:1 ratio of Lorentzian to Gaussian contribution for the pre-edge feature successfully reproduced these spectral features.

The number of functions employed to fit the rising edge background was chosen on the basis of features clearly indicated by the second derivative of the data. These rising edge functions were pseudo-Voigt line shapes for which the Gaussian:Lorentzian mixture was allowed to vary to give the best empirical fit. In all cases the minimum number of functions required to successfully reproduce the data was utilized.

Fits used in the calculation of pre-edge peak intensity were optimized to reproduce both the data and the second derivative of the data. For each spectrum, a number of fits which reproduced both the data and the second derivative of the data were obtained. Fits were performed over several energy ranges: from one which included just the tail of the rising edge, to one which included the white line maximum of the edge. The value reported for the intensity of a pre-edge feature (where peak area was approximated by the height × full-width-at-half-maximum (fwhm)) is the average of all the pseudo-Voigts which successfully fit the feature. For each sample, the standard deviation of the average of the areas was calculated to quantitate the uncertainty of the fit.

E. Determination of Rising Edge Positions. The energies reported for the rising edge position were determined from the highest energy maximum in the first derivative of the data in the rising edge region. These measurements were performed independently of the above described fitting procedures.

F. Error Analysis. There are several possible sources of systematic error in the analysis of these spectra. Normalization procedures can introduce a 1−3% difference in pre-edge peak heights, as determined by varying the parameters used to normalize a set of Cl K-edge spectra such that the final fits met requirements of consistency. This maximum of ~3% error and the error resulting from the fitting procedure discussed above were taken into account in the calculation of pre-edge intensities and subsequent determinations of covalency. Experimental self-absorption could, in principle, result in an artificially low observed intensity. However, care was taken to avoid self-absorption in these experiments (*vide supra*), and this effect is assumed to be negligible.

The uncertainty in pre-edge and edge energies is limited by the reproducibility of the edge spectra (~0.1 eV). Thus, relative energies of features are reported with an error of ± 0.1 eV. For the purposes of the energy analyses herein, no error has been assumed for the $10Dq$ ligand field splittings used to quantitate energy shifts of metal d-derived orbitals.

G. SCF-Xα-SW Calculations. The calculation of D_{2d} $CuCl_4^{2-}$ has been described previously,[21] and only the most salient details of the calculation are included here. Standard SCF-Xα-SW calculations[22] on T_d MCl_4^{n-} molecules (M = Ni^{II}, Co^{II}, Fe^{II}, and Fe^{III}) were performed on DECstation 3100 computers with ~300 iterations required for convergence. The calculations were considered to have converged when the largest relative change in the potential between subsequent iterations was less than 10^{-3}. Bond distances used in the calculations were adapted from crystal structure values: Cu−Cl = 2.230,[11] Ni−Cl = 2.270,[23] Co−Cl = 2.280,[24] Fe^{II}−Cl = 2.291,[25] and Fe^{III}−Cl = 2.185 Å.[26] The α values of Schwarz[27] and maximum l values of 4, 3, and 2 were used for the outer sphere, the metal, and the chloride, respectively. A Watson sphere coincident with the outer sphere radius was used in calculations of these charged species. Sphere radii for divalent metal calculations were chosen to be the same as those in the D_{2d} $CuCl_4^{2-}$ calculation which were optimized to match experimental g-values[21] (M^{II} = 3.11, Cl = 2.49 bohrs). The sphere radii for the $Fe^{III}Cl_4^-$ calculation were chosen such that the metal sphere radius was slightly smaller (2.90 bohrs) than that in the divalent calculations, consistent with a contraction of the metal sphere and decrease in bond length upon increase in oxidation state. The chloride radii were the same (2.49 bohrs) as those in the other calculations.

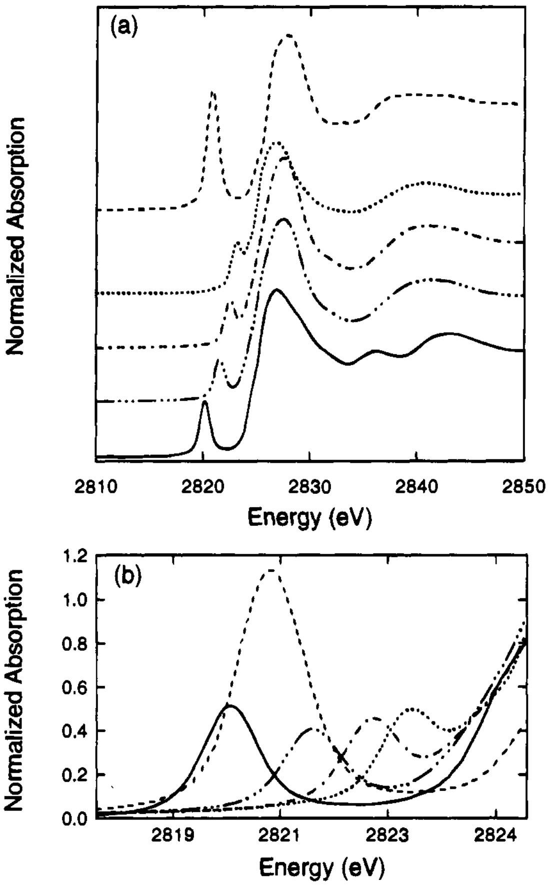

Figure 1. Cl K-edge XAS spectra of the T_d complexes $CuCl_4^{2-}$ (—), $NiCl_4^{2-}$ (— · · ·), $CoCl_4^{2-}$ (- · · -), $Fe^{II}Cl_4^{2-}$ (· · ·), and $Fe^{III}Cl_4^-$ (- - -). The entire edge region of each spectrum is shown in (a). Each spectrum exhibits a pre-edge feature, which is shown on an expanded scale in (b).

Results

The Cl K-edge X-ray absorption spectra of the ~T_d complexes MCl_4^{n-} (M = Cu^{II}, Ni^{II}, Co^{II}, Fe^{II}, and Fe^{III}) are shown in Figure 1a. Each spectrum exhibits a pre-edge feature in the 2819−2824 eV range which is shown expanded in Figure 1b. Over the divalent series, the energies of the pre-edge features vary in the order $Cu^{II} < Ni^{II} < Co^{II} < Fe^{II}$. The $CuCl_4^{2-}$ pre-edge is lowest in energy at 2820.2 eV, and the $Fe^{II}Cl_4^{2-}$ pre-edge is at highest energy, appearing as a shoulder on the rising edge at 2823.1 eV. The $Fe^{III}Cl_4^-$ pre-edge is at much lower energy than that of the ferrous complex, appearing as a well-resolved peak at 2820.8 eV. The rising edge energy positions in the spectra in Figure 1a are observed at 2825.0 eV for $Ni^{II}Cl_4^{2-}$, $Co^{II}Cl_4^{2-}$, and $Fe^{II}Cl_4^{2-}$ and at 2825.4 and 2826.0 eV for $Cu^{II}Cl_4^{2-}$ and $Fe^{III}Cl_4^-$, respectively.

The $CuCl_4^{2-}$ pre-edge is the most intense of those exhibited by the divalent centers, with the Ni^{II}, Co^{II}, and Fe^{II} centers having approximately the same pre-edge intensity, within experimental error. The pre-edge of $Fe^{III}Cl_4^-$ is more than 3 times as intense as that of the ferrous complex. Table 2

---

[19] Tyson, T. A.; Roe, A. L.; Frank, P.; Hodgson, K. O.; Hedman, B. *Phys. Rev. B* **1989**, *39A*, 6305−6315.

[20] Lytle, F. W. In *Applications of Synchrotron Radiation*; Winick, H., Xian, D., Ye, M. H., Huang, T., Eds.; Gordon & Breach: New York, 1989; pp 135.

[21] Gewirth, A. A.; Cohen, S. L.; Schugar, H. J.; Solomon, E. I. *Inorg. Chem.* **1987**, *26*, 1133−1146.

[22] Cook, M.; Case, D. A. *QCPE Program #465* **1991**, *23*, 21−22.

[23] Pauling, P. *Inorg. Chem.* **1966**, *5*, 1498−1505.

[24] Both the Ni and Co complexes used in this study have the same counterion. Since the Co−Cl bond distance is not known,[23] the Co−Cl bond length was set to the Ni−Cl distance +0.01Å based on the fact that in the (Et_4N) and (Me_4N) salts, the Co−Cl bond length was ~0.01−0.02 Å longer than the Ni−Cl distance.

[25] Lauher, J. W.; Ibers, J. A. *Inorg. Chem.* **1975**, *14*, 348−352.

[26] Cotton, F. A.; Murillo, C. A. *Inorg. Chem.* **1975**, *14*, 2467−2469.

[27] Schwarz, K. *Phys. Rev. B* **1972**, *5*, 2466−2468.

Table 2. MCl_4^{n-} Cl K-Edge Pre-edge Energies and Intensities and Rising Edge Inflection Points

complex	pre-edge energy[a] (eV)	pre-edge intensity[b]	rising edge inflection[c] (eV)
$CuCl_4^{2-}$	2820.2	0.526 ± 0.017	2825.4
$NiCl_4^{2-}$	2821.5	0.428 ± 0.017	2825.0
$CoCl_4^{2-}$	2822.5	0.419 ± 0.021	2825.0
$Fe^{II}Cl_4^{2-}$	2823.1	0.427 ± 0.039	2825.0
$Fe^{III}Cl_4^{-}$	2820.8	1.505 ± 0.064	2826.0

[a] The error in these energies, as determined from the standard deviation of fits to the data, is ≤±0.009 eV. [b] Reported error is the standard deviation of the area as determined from fits to the data and the ~3% error from normalization of the data. [c] Error in the inflection point is <±0.1 eV; the inflection point reported is the highest energy feature in the first derivative in the rising edge region.

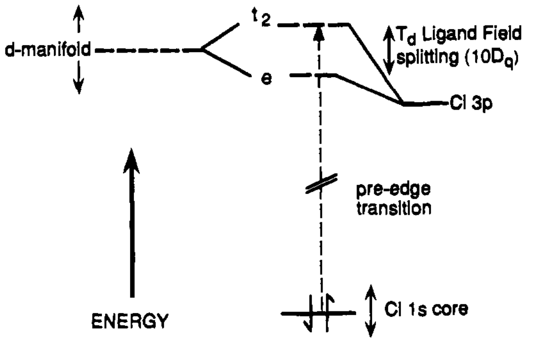

Figure 2. Schematic representation of the contributions to the energy of the pre-edge feature in T_d metal complexes. The pre-edge energy is determined by the Cl 1s core energy and the energy of the metal d-derived orbitals. The metal d-type orbital energy derives from the energy of the d-manifold and the ligand field splitting of the d-orbitals. The dashed arrow depicts a pre-edge transition to the t_2-set of orbitals.

summarizes the quantitative energy and intensity of each pre-edge feature as well as the inflection point of the edge for each spectrum.

Analysis

I. Pre-edge Energies. Figure 2 shows an energy level diagram depicting a transition (in this case to the t_2-set of orbitals) which gives rise to the pre-edge feature. As seen in Figure 2, a combination of factors affect the energy position of a pre-edge transition.[9] A shift in the core Cl 1s energy, which is related to the relative charge on the chloride, results in a change in the observed pre-edge energy. More charge donation to the metal results in a shift in the ligand core to deeper binding energy and a shift to higher energy of transitions from the Cl 1s core orbital. In addition, the energy of the pre-edge transition depends on the metal d-derived orbital energy, which has two contributions. First, the strength of the ligand field of the complex determines the d-orbital energy splitting ($10Dq$) and thus contributes to the metal d-derived orbital energy. Second, the overall d-manifold can shift in energy. This is related to the oxidation state and effective charge on the metal (which affects the energy of all the metal orbitals) and is also related to the coordination number of the metal (the total antibonding and repulsive interactions with the ligands), which is constant over the series examined herein. Quantitative estimates of the relative Cl 1s core energy and the ligand field contribution to metal d-derived orbital energy can be obtained (*vide infra*), and by correction of the observed pre-edge energy for these effects, the contribution to the pre-edge energy from energy shifts of the d-manifold can be determined.

The intense electric dipole-allowed transition observed at the onset of the edge jump is a Cl 1s → 4p transition. The energy of this main edge transition is determined from the rising edge inflection point. Shifts in this energy directly reflect shifts in the Cl 1s core level in response to the relative charge on the atom with the rising edge energy being lower for a more negatively charged ligand.[9] Table 3 gives the positions of the rising edge inflection points of each Cl K-edge spectrum relative to that of $CuCl_4^{2-}$. The relationship between rising edge position and chloride charge has been derived[9] from a series of compounds whose charges were determined experimentally from Auger spectroscopy. This relationship can be applied to these data to obtain an estimate of the charge on the chloride ligand in each complex. The charge calculated for the chloride in $CuCl_4^{2-}$ is −0.54 and in $Fe^{III}Cl_4^{-}$ is −0.33, with the chloride in Ni^{II}, Co^{II}, and Fe^{II} complexes having a charge of −0.65 (see Table 3).

In Cu^{II}, Ni^{II}, and Co^{II} there are only vacancies in the t_2-set of the T_d orbitals; thus, only transitions to the t_2-set contribute to pre-edge intensity. The ligand field (LF) contribution to the pre-edge energy can be estimated from $^2/_5$ the value of $10Dq$ (the LF splitting of the t_2 orbitals relative to the d-manifold energy, see Figure 2). The value of $10Dq$ has been determined from analysis of the LF spectrum of each complex. The $10Dq$ value used in this analysis is that of the one-electron reduced (d^{n+1}) metal ion excited state, which is expected to be ~60% of the splitting in the ground state.[28] The ground state and excited state $10Dq$ splittings are given in Table 3. For $CuCl_4^{2-}$, the distortion from T_d to D_{2d} has a non-negligible effect on the metal d-derived orbital energies, splitting the t_2-set into e + b_2, where b_2 is the higher-lying, half-occupied orbital to which the pre-edge transition occurs. The additional b_2−e splitting is estimated from Xα calculations on the site (see Supplementary Table S6) and is given in Table 3.

For Fe^{III} and Fe^{II} tetrachlorides, transitions to both the e-set and t_2-set of T_d orbitals contribute to the pre-edge intensity. The shift of the pre-edge energy due to LF effects must then be calculated from theoretical energy and intensity ratios. In the Analysis, section II (part C), we find for $Fe^{III}Cl_4^{-}$ that the pre-edge transition to the e-set is at 2820.5 eV while the transition to the t_2-set is at 2821.0 eV. The splitting between them corresponds to the excited state d^{n+1} $10Dq$. Since the e-set is at lower energy than the d-manifold by $-^3/_5$ $10Dq$ (see Figure 2), the d-manifold energy is at 2820.8 eV. The center of the observed pre-edge feature (which contains contributions from both types of transitions) is also at 2820.8 eV (Table 3). Thus, the effect of the ligand field on the observed pre-edge feature energy is negligible. For $Fe^{II}Cl_4^{2-}$, the pre-edge transition to the e-set is found to be at 2822.8 eV (see Analysis, section II (part C)). By use of excited state $10Dq$ values, the d-manifold energy is calculated as in $Fe^{III}Cl_4^{-}$ to be 2823.0 eV, indicating that the ligand field contribution to the pre-edge feature energy is 0.10 eV since the pre-edge feature appears at 2823.1 eV in the experimental data. The ground state and excited state $10Dq$ splittings for $Fe^{III}Cl_4^{-}$ and $Fe^{II}Cl_4^{2-}$ are given in Table 3, in addition to the magnitude of the LF contribution to the pre-edge energy relative to $CuCl_4^{2-}$ for each MCl_4^{n-} complex.

The relative energy shifts in the Cl 1s core and the metal d-derived orbitals can now be used to obtain pre-edge energies which have been LF- and core-shift-corrected. Shifts in the metal d-derived orbital energy due to LF effects are subtracted from, and the core 1s energy are added to, the observed pre-edge transition energy (see Figure 2).[9] These corrected pre-edge energies are given in Table 3. If these were the only contributions to the pre-edge energy, the corrected energy would be 2820.2 eV, the pre-edge energy for $CuCl_4^{2-}$, which has been

---

(28) Karshipin, T. B.; Gebhard, M. S.; Solomon, E. I.; Raymond, K. N. J. Am. Chem. Soc. **1991**, *113*, 2977–2984.

Table 3. Cl K-Edge Energy Analysis Parameters

					ligand field induced HOMO shift (eV)[h]			
complex	calc. charge	Cl 1s core energy shift relative to $CuCl_4^{2-}$ (eV)[a]	ground state 10*Dq* (cm^{-1})	excited state 10*Dq* (cm^{-1})[g]	absolute	relative to $CuCl_4^{2-}$	corrected pre-edge energy (eV)[i]	relative d-manifold energy shift (eV)
$CuCl_4^{2-}$	−0.54	0	4160/4436[b]	2496/2662[b]	0.34	0	2820.2	0
$NiCl_4^{2-}$	−0.65	+0.4	3600[c]	2160	0.10	0.24	2821.7	1.5
$CoCl_4^{2-}$	−0.65	+0.4	3000[d]	1800	0.09	0.25	2822.6	2.4
$Fe^{II}Cl_4^{2-}$	−0.65	+0.4	4100[e]	2460	0.10	0.24	2823.3	3.1
$Fe^{III}Cl_4^{-}$	−0.33	−0.6	6500[f]	3900	~0	0.34	2819.9	−0.3

[a] Determined from experimental rising edge inflection points. Error for these energy differences is estimated to be ±0.1 eV. [b] Gewirth, A. A.; Cohen, S. L.; Schugar, H. J.; Solomon, E. I. *Inorg. Chem.* **1987**, *26*, 1133−1146. Values reported for $CuCl_4^{2-}$ are the 10*Dq* splitting and the D_{2d} splitting of the b_2 and e orbitals (see also supplementary Table S6). [c] Goodgame, D. M. L.; Goodgame, M.; Cotton, F. A. *J. Am. Chem. Soc.* **1961**, *83*, 4161−4167. [d] Cotton, F. A.; Goodgame, D. M. L.; Goodgame, M. *J. Am. Chem. Soc.* **1961**, *83*, 4690−4699. [e] Furlani, C.; Cervone, E.; Valenti, V. *J. Inorg. Nucl. Chem.* **1963**, *25*, 159−163. [f] Deaton, J. C.; Gebhard, M. S.; Solomon, E. I. *Inorg. Chem.* **1989**, *28*, 877−889. [g] The excited state 10*Dq* will be approximately 60% of the ground state value.[28] [h] The shift to higher energy of the pre-edge energy due to ligand field effects is equal to $^2/_5(10Dq) + {}^2/_3(b_2{-}e \text{ splitting})$ for Cu^{II} and $^2/_5(10Dq)$ for Ni^{II} and Co^{II}. For Fe^{II} and Fe^{III} the displacement can be estimated from the energy of the transition to the e-set (*vide infra* and see Figure 4, parts d and e). [i] The corrected pre-edge energy is obtained by subtracting the relative LF shift and adding the relative Cl 1s core shift (see text).

Table 4. Ground States and Group Theoretically-Allowed Excited States for MCl_4^{n-} Pre-edge Transitions

complex	ground d^n	ground configuration (holes)	ground state	excited configuration (holes)[a]	parent d^{n+1} excited state	allowed excited state (from ligand a_1)	allowed excited state (from ligand t_2)
$CuCl_4^{2-}$	d^9	t_2	$^2T_2$	t_2^0	$^1A_1$	$^2A_1$	$^2T_2$
$NiCl_4^{2-}$	d^8	t_2^2	$^3T_1$	t_2^1	$^2T_2$	$^3T_2$	$^3E + {}^3T_1 + {}^3T_2$
$CoCl_4^{2-}$	d^7	t_2^3	$^4A_2$	t_2^2	$^3T_1$[b]	$^4T_1$	$^4T_1$
$Fe^{II}Cl_4^{2-}$	d^6	et_2^3	^5E	t_2^3	$^4A_2$		$^5T_1$
				et_2^2	$^4T_2$	$^5T_2$	$^5T_1 + {}^5T_2$
					$^4T_1$[b]	$^5T_1$	$^5T_1 + {}^5T_2$
$Fe^{III}Cl_4^{-}$	d^5	$e^2t_2^3$	$^6A_1$	et_2^3	^5E		$^6T_2$
				$e^2t_2^2$	$^5T_2$	$^6T_2$	$^6T_2$

[a] Excited state configurations are given in the strong field limit. [b] States for which intermediate ligand field mixing with higher lying states of the same symmetry is possible.

used as the reference compound. Deviations from this value indicate that an additional effect, the overall energy of the d-manifold, must be taken into account. Table 3 (last column) gives the relative deviation in the corrected pre-edge energy (from 2820.2 eV), which is attributable to a d-manifold energy shift. The d-manifold energies vary in the order $Fe^{III} < Cu^{II} < Ni^{II} < Co^{II} < Fe^{II}$.

These d-manifold shifts are consistent with the periodic trend in the effective nuclear charge (Z_{eff}) on each metal. As the metal Z_{eff} increases across the first row of the periodic table for the divalent series (from Fe^{II} to Cu^{II}), there is a shift in the d-manifold to deeper binding energy. The d-manifold in $Fe^{III}Cl_4^-$ is also significantly deeper in energy than in $Fe^{II}Cl_4^{2-}$, due to oxidation of the iron. Note that over the series in Figure 1, the contribution to the pre-edge energy from the shift in d-manifold energy is much larger in each case than the contributions from the LF repulsion and the shift in the Cl 1s core energy.

II. Pre-edge Intensities. In this section the methodology is developed for relating pre-edge intensity to covalency in metal d-derived orbitals for metal systems with more than one hole. The theory is developed first and then applied to the experimental data, each part proceeding in several steps. In part A, strong field group theoretical predictions of possible one-electron pre-edge transitions are made. In part B, the irreducible tensor method is used to derive dipole strength expressions which describe the intensity of the transitions in the strong field limit. Mixing of excited states in intermediate-strength ligand fields can redistribute pre-edge intensity to higher energy. In part C, the degree of this mixing is calculated for each complex, along with the ligand field energy splittings and intensity ratios for each contributing pre-edge transition. In part D, these energy splittings and intensity ratios are applied to the experimental spectra to determine the total pre-edge transition intensity for each complex. The theoretical dipole strength expressions from part B are then applied to these data to obtain an estimate of ligand−metal covalency. Finally, Xα calculations of these complexes are presented in part E and compared to the experimental results.

A. Pre-edge Transitions in the Strong Field Limit. In order to extract information from the pre-edge transition intensity, the transitions must first be assigned. In systems with more than one d-hole, multiplet effects require that the pre-edge transitions be described in terms of many-electron states. Table 4 gives the many-electron (d^n) ground configuration and ground state for each molecule. The one-electron excited states are derived from the d^{n+1} metal ion *parent*, which has the electron excited into the t_2 or e orbital. The ligand 1s orbitals on the four chloride ligands form an $a_1 + t_2$-set with respect to the T_d molecular symmetry. The complete final excited state then involves coupling the ligand hole (a_1 or t_2) with the d^{n+1} parent excited state. Only parent states which, after coupling in the ligand hole, result in spin and electric dipole-allowed final states are considered. Table 4 gives, for the strong field limit, these parent excited states and the electric dipole-allowed total final states, which include the ligand core hole. $CuCl_4^{2-}$, $NiCl_4^{2-}$, and $CoCl_4^{2-}$ each have only one parent excited state ($^1A_1$, $^2T_2$, and $^3T_1$, respectively). $Fe^{III}Cl_4^-$ has two excited parents states, ^5E and $^5T_2$, corresponding to transitions to the e- and t_2-set, respectively. $Fe^{II}Cl_4^{2-}$ has one excited parent state ($^4A_2$) arising from a transition to the e-set as well as two excited parent states arising from a transition to the t_2-set ($^4T_1 + {}^4T_2$).

B. Multiplet Contributions to Intensity in the Strong Field Limit. In order to extract information about ligand−metal covalency from spectra of complexes with more than one d-manifold hole, the intensity of allowed pre-edge transitions

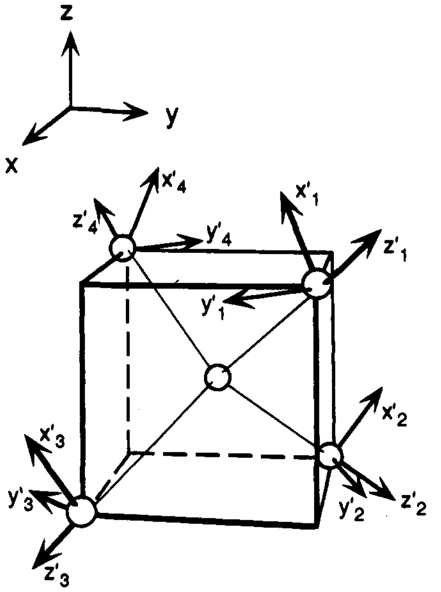

Figure 3. The T_d molecular axis system and ligand p-orbital vectors used for molecular orbital construction (from Ballhausen, C. J.; Gray, H. B. *Molecular Orbital Theory*; Benjamin Press: New York, 1964; pp 108–109). The molecular axes are x, y, z, and the local axis system of each ligand is designated with x', y', z'. For each ligand, the z' (σ-bonding) p orbital is along the ligand–metal bond. The π-bonding orbitals are perpendicular to the bond with each y' being 90° to the molecular z-axis. Note that the x' and y' vectors of ligand centers 1 and 4 are related by symmetry as are centers 2 and 3, but the two sets of vectors do not directly transform into one another with point group operations.

(see Table 4) must be related to the amount of Cl 3p character in the one-electron t_2 and e orbitals. This relationship can be derived by describing the pre-edge intensity in terms of the dipole strength (D_o), given in eq 2, and evaluating the dipole strength in a form which includes the one-electron molecular orbitals.

$$D_o = \frac{1}{3|A|}\sum_{\alpha i\beta}|\langle A\alpha|\mathbf{r}_i|B\beta\rangle|^2 \qquad (2)$$

A and B are the many-electron ground and excited states, respectively, $|A|$ is the degeneracy of the ground state, $\mathbf{r}_i$ is the electric dipole operator, and α, i, and β are components of the ground state, dipole operator, and excited state, respectively. Equation 2 can be evaluated by construction of all the ground and excited state wavefunctions for each metal center. This is an involved and lengthy procedure. This study has employed an alternative approach, the irreducible tensor method,[29] which uses the Wigner–Eckart theorem to take advantage of symmetry to simplify the problem.

The first step in the application of the irreducible tensor method is the expansion of each pre-edge transition integral with respect to the components of the ground state, excited state, and the electric dipole operator, which transforms as T_2 in T_d symmetry. Each expanded integral is evaluated to determine whether it is nonzero by group theory. In subsequent steps the number of matrix elements which must actually be evaluated is reduced by converting each nonzero integral first to a many-electron reduced matrix element and then to a one-electron reduced matrix element, each being independent of the components of the many-electron states or of the one-electron orbitals. As a result of the analysis for the T_d MCl_4^{n-} systems, each many-electron integral reduces to one of three one-electron-reduced matrix elements: $\langle a_1||t_2||t_2\rangle$, $\langle t_2||t_2||t_2\rangle$, and $\langle t_2||t_2||e\rangle$. The details of the construction of reduced matrix elements for this analysis are given in section I of the Appendix and in Supplementary Table S1.

Each one-electron reduced matrix element can be related to a real one-electron integral of the form, $\langle a\alpha|\mathbf{r}|b\beta\rangle$, where $|a\alpha\rangle$ and $|b\beta\rangle$ are one-electron orbitals for which α and β designate the specific one-electron orbitals of symmetry a and b, respectively; and $\mathbf{r}$ is the electric dipole operator. The integral $\langle a\alpha|\mathbf{r}|b\beta\rangle$ is evaluated using symmetry-adapted linear combinations (SALC's) of atomic orbitals for one-electron molecular orbital wavefunctions. The SALC's used in this evaluation are based on the T_d geometry and ligand 3p-vectors defined in Figure 3. The molecular axis system is designated x, y, z, and the local axis system of each ligand is designated x', y', z', with z' along the metal–ligand bond. The linear combinations of Cl 1s orbitals, as well as the t_2 and e one-electron valence orbitals (which contain both metal 3d- and ligand 3p-character) are given in Table 5. The coefficients c_1 and c_2 describe the ligand $3p_\sigma$ and $3p_\pi$ contributions to the t_2-set, respectively, while the c_3 coefficient reflects the ligand $3p_\pi$ character in the e-set. For one-electron molecular orbitals, $a\alpha$ and $b\beta$, written as $a\alpha = C_M\chi_M + C_L\chi_L$, where χ_M and χ_L are the symmetry-adapted metal and ligand combinations given in Table 5, the evaluation of the real one-electron matrix elements, $\langle a\alpha|\mathbf{r}|b\beta\rangle$, involves the expansion given by eq 3, where the prime indicates the $b\beta$ component

$$\langle a\alpha|\mathbf{r}|b\beta\rangle = C_M C_{M'}\langle\chi_M|\mathbf{r}|\chi_{M'}\rangle + C_M C_{L'}\langle\chi_M|\mathbf{r}|\chi_{L'}\rangle + C_L C_{M'}\langle\chi_L|\mathbf{r}|\chi_{M'}\rangle + C_L C_{L'}\langle\chi_L|\mathbf{r}|\chi_{L'}\rangle \qquad (3)$$

The expansion includes metal–metal, metal–ligand, and ligand–ligand terms. It has been determined for ligand-to-metal charge transfer (LMCT) transitions that the ligand–ligand term gives the dominant contribution to $\langle a\alpha|\mathbf{r}|b\beta\rangle$.[30–32] For LMCT transitions, this ligand–ligand term is further rewritten in the dipole approximation according to eq 4,

$$\langle\chi_L|\mathbf{r}(x,y,z)|\chi_{L'}\rangle = p\mathrm{R}\langle \mathrm{s}|\mathbf{r}(x',y',z')|\mathrm{p}\rangle \qquad (4)$$

where $\mathbf{r}(x,y,z)$ is the electric dipole operator in the molecular axis frame, and $\mathbf{r}(x',y',z')$ is the electric dipole operator in the ligand axis frame; $\langle \mathrm{s}|\mathbf{r}(x',y',z')|\mathrm{p}\rangle$ is a pure ligand s → p transition, localized on the ligand; and pR is the projection of the ligand axis frame, at the distance R from the metal center, onto the electric dipole vector. This approximation should be particularly good for ligand pre-edge transitions due to the localized nature of the ligand 1s orbital involved in the transition. The details of the evaluation of one-electron integrals and their relation to the one-electron reduced matrix elements of this analysis are given in section II of the Appendix and in Supplementary Tables S2–S4.

The final step of the analysis is the determination of the dipole strength for each transition. This requires the summation, given by eq 2, of the square of each matrix element in terms of the one-electron integrals which have been evaluated with symmetry-adapted molecular orbitals. The electron repulsion between a localized ligand core (1s) hole and electrons in the valence d-manifold is minimal. As a result, transitions to excited states which are related to the same d^{n+1} parent, differing only in the ligand core orbital of origin (a_1 or t_2), should be degenerate, and contributions from their dipole strengths are

---

(29) Griffith, J. S. *The Irreducible Tensor Method for Molecular Symmetry Groups*; Prentice-Hall: Englewood Cliffs, NJ, 1962; pp 1–427.

(30) Van Der Avoird, A.; Ros, P. *Theor. Chim. Acta* **1966**, *4*, 13–21.

(31) Wiers, B. H.; Reynolds, W. L. *Inorg. Chem.* **1966**, *5*, 2016–2021.

(32) Bird, B. D.; Day, P. *J. Chem. Phys.* **1968**, *49*, 392–403.

Table 5. Symmetry-Adapted One-Electron Wavefunctions for a T_d Molecule[a]

ligand core 1s orbitals	SALC's
a_1	$^1/_2(s_1 + s_2 + s_3 + s_4)$
$t_2(x)$	$^1/_2(s_1 - s_2 + s_3 - s_4)$
$t_2(y)$	$^1/_2(s_1 + s_2 - s_3 - s_4)$
$t_2(z)$	$^1/_2(s_1 - s_2 - s_3 + s_4)$

metal d-type orbitals	SALC's metal component	ligand component
$e(\theta)$	$\sqrt{[1 - c_3^2]}d_{z^2}$	$+ c_3\,[^1/_2(p_{x'1} - p_{x'2} - p_{x'3} + p_{x'4})]$
$e(\epsilon)$	$\sqrt{[1 - c_3^2]}d_{x^2-y^2}$	$+ c_3\,[^1/_2(p_{y'1} - p_{y'2} - p_{y'3} + p_{y'4})]$
$t_2(x)$	$\sqrt{[1 - (c_1^2 + c_2^2)]}d_{yz}$	$+ c_1\,[^1/_2(p_{z'1} - p_{z'2} + p_{z'3} - p_{z'4})] + c_2\,[^1/_4[(p_{x'1} + p_{x'2} - p_{x'3} - p_{x'4}) + \sqrt{3}(-p_{y'1} - p_{y'2} + p_{y'3} + p_{y'4})]]$
$t_2(y)$	$\sqrt{[1 - (c_1^2 + c_2^2)]}d_{xz}$	$+ c_1\,[^1/_2(p_{z'1} + p_{z'2} - p_{z'3} - p_{z'4})] + c_2\,[^1/_4[(p_{x'1} - p_{x'2} + p_{x'3} - p_{x'4}) + \sqrt{3}(p_{y'1} - p_{y'2} + p_{y'3} - p_{y'4})]]$
$t_2(z)$	$\sqrt{[1 - (c_1^2 + c_2^2)]}d_{xy}$	$+ c_1\,[^1/_2(p_{z'1} - p_{z'2} - p_{z'3} + p_{z'4})] - c_2\,[^1/_2(p_{x'1} + p_{x'2} + p_{x'3} + p_{x'4})]$

[a] Taken from Ballhausen, C. J.; Gray, H. B. *Molecular Orbital Theory*; Benjamin Press: New York, 1964; pp 108–109.

Table 6. Strong Field Dipole Strength Expressions for MCl_4^{n-} Pre-edge Transition Intensities

complex	parent d^{n+1} excited state	dipole strength for transition to parent excited state
$CuCl_4^{2-}$	$^1A_1$	$^1/_3(c_1^2 + c_2^2)R^2\langle s\|\mathbf{r}\|p\rangle^2$
$NiCl_4^{2-}$	$^2T_2$	$^2/_3(c_1^2 + c_2^2)R^2\langle s\|\mathbf{r}\|p\rangle^2$
$CoCl_4^{2-}$	$^3T_1$	$(c_1^2 + c_2^2)R^2\langle s\|\mathbf{r}\|p\rangle^2$
$Fe^{II}Cl_4^{2-}$	$^4A_2$	$(^1/_3)c_3^2R^2\langle s\|\mathbf{r}\|p\rangle^2$
	$^4T_2$	$(^1/_2)(c_1^2 + c_2^2)R^2\langle s\|\mathbf{r}\|p\rangle^2$
	$^4T_1$	$(^1/_2)(c_1^2 + c_2^2)R^2\langle s\|\mathbf{r}\|p\rangle^2$
$Fe^{III}Cl_4^{-}$	^5E	$(^2/_3)c_3^2R^2\langle s\|\mathbf{r}\|p\rangle^2$
	$^5T_2$	$(c_1^2 + c_2^2)R^2\langle s\|\mathbf{r}\|p\rangle^2$

additive. For example, the $^2A_1$ and $^2T_2$ excited states of T_d $CuCl_4^{2-}$ arise from the same parent excited state ($^1A_1$) and thus contribute to pre-edge intensity at the same energy. The details of the final summation for the dipole strength for each d^{n+1} parent excited state are given in section III of the Appendix and in Supplementary Table S5.

The resulting expressions for the total sum dipole strength for each d^{n+1} parent excited state are given in Table 6. For Cu^{II}, Ni^{II}, and Co^{II}, in which there is only one parent excited state, the intensity of the transition to each state is proportional to the sum of the σ and π 3p-covalency in the t_2-set $[c_1^2 + c_2^2]$, a constant related to the number of ground state t_2-set holes, the square of the bond length, and the intensity of a pure Cl 1s → 3p transition ($\langle s|\mathbf{r}|p\rangle^2$). It should be noted that the result obtained for T_d $CuCl_4^{2-}$ holds even if the symmetry is lowered to D_{2d}.[33] Further, the expression derived for the Cu^{II} complex by this methodology is exactly analogous to that given in the Introduction for the simple 1s → ψ^* transition.

For $Fe^{III}Cl_4^-$, there is one parent excited state arising from a transition to the e-set (^5E) and one parent excited state derived from a transition to the t_2-set ($^5T_2$). The dipole strength expression for the transition to the $^5T_2$ parent is identical to that for the single Co^{II} excited state parent because both metal sites have the same ground state t_2 configurations. The intensity of the transition to the ^5E parent excited state is proportional to the π 3p-covalency $[c_3^2]$ in the e-set and to a constant related to the number of ground state e-set holes.

For $Fe^{II}Cl_4^{2-}$, there is one parent excited state arising from a transition to the e-set ($^4A_2$) and two parent excited states derived from a transition to the t_2-set ($^4T_2 + {}^4T_1$). The dipole strengths of the pre-edge transitions to the $^4T_2$ and $^4T_1$ parents are equal, and each is half the value calculated for $CoCl_4^{2-}$. Thus, for transitions to the t_2-set, $Fe^{II}Cl_4^{2-}$ has the same total dipole strength as $CoCl_4^{2-}$ because Co^{II} and Fe^{II} have the same t_2 ground configuration. However, the intensity in $Fe^{II}Cl_4^{2-}$ is distributed equally over two excited states. The intensity of the transition to the $^4A_2$ parent in $Fe^{II}Cl_4^{2-}$ is related to that for the ^5E parent in Fe^{III}, with the difference reflecting the fact that Fe^{II} has one less e-hole in the ground state.

C. Higher State Mixing and Excited State Energies in Intermediate-Strength Ligand Fields. The analysis of pre-edge intensities has up to this point treated the transitions in the strong field limit. For a T_d complex with chloride ligands, however, the treatment must be extended to account for the fact that these complexes are closer to the weak field limit. In intermediate-strength ligand fields, mixing between states of appropriate symmetry is non-negligible. Mixing of a pre-edge transition parent excited state with a higher lying d^{n+1} excited state will result in the redistribution of pre-edge intensity to higher energy. The consequence of this mixing would then be a reduction in the experimentally observed pre-edge intensity.

Both Co^{II} and Fe^{II} have d^{n+1} parent excited states which can mix with higher lying states of appropriate symmetry. These higher lying excited states derive from formally forbidden two-electron excitations. This mixing will redistribute some of the intensity predicted by the strong field dipole strength (for the transition to the allowed d^{n+1} parent (Table 6)) to higher energy (relative to the pre-edge transition in Figure 1). The magnitude of this mixing is determined from the d^{n+1} Tanabe–Sugano matrices[34] for Co^{II} and Fe^{II}, assuming reasonable values of Dq and B for the d^{n+1} excited states. As described in the Analysis, section I, the excited state Dq is expected to be approximately 60% of the ground state value.[28] Appropriate values of B are obtained from values for F_2 determined for the d^{n+1} free ions Co^I and Fe^I [35] and using $F_4 = 0.07F_2$ and $B = F_2 - 5F_4$. Table 7 gives excited state values of Dq and B, as well as the coefficients of mixing calculated from the Tanabe–Sugano matrices, and the absolute and relative energy splittings of excited states for T_d $Co^{II}Cl_4^{2-}$ and $Fe^{II}Cl_4^{2-}$. Because the magnitude of B might be expected to be further reduced due to covalency, the B values in Table 7 should be taken as an upper limit. For smaller B, there would be less mixing between the two states and a smaller energy splitting.

For $Co^{II}Cl_4^{2-}$, the pre-edge intensity for the transition to the

---

[33] That the dipole strength obtained for T_d $CuCl_4^{2-}$ is equivalent to that for D_{2d} $CuCl_4^{2-}$ is described in detail in the Appendix, section IV.

[34] Dunn, T. M.; McClure, D. S.; Pearson, R. G. *Some Aspects of Crystal Field Theory*; Harper & Row: New York, 1965; pp 42–45.

[35] Ferguson, J. *Prog. Inorg. Chem.* **1970**, *12*, 159–293.

Table 7. Distribution of Energies and Intensities for Final States of MCl_4^{n-} Pre-edge Transitions

T_d metal ion[a]	parent d^{n+1} excited state	higher state of appropriate symmetry for mixing	excited state Dq (cm^{-1})	excited state B (cm^{-1})	calculated energy value[b] (cm^{-1})	relative energy value (eV)	coeff of mixing[b]	ratios from strong field D_o[c]	theoretical intensity ratios[d]
Co^{II}	$^3T_1{}^a$		186	812	−6165.5	0	0.84	1	1
		$^3T_1{}^b$			+7213.5	1.66	0.16	1	0.19
Fe^{II}	$^4A_2$		250	722	−13830.0	−0.31		$(^1/_3)c_3^2$	0.42
	$^4T_2$				−11330.0	0		$^1/_2(c_1^2 + c_2^2)$	1
	$^4T_1{}^a$				−9436.0	0.23	0.29	$^1/_2(c_1^2 + c_2^2)$	0.29
		$^4T_1{}^b$			+106.0	1.42	0.71		0.71
Fe^{III}	^5E		393			0		$(^2/_3)c_3^2$	0.58
	$^5T_2$					0.49		$(c_1^2 + c_2^2)$	1

[a] Cu and Ni are not included here because there is only one parent excited state in each case; thus, there is no splitting to be calculated. [b] Calculated using Tanabe−Sugano matrices.[34] [c] See Table 6. [d] The ratios between transitions to t_2 orbitals are completely determined from the calculated D_o expressions and the calculated coefficients of mixing. The ratios between transitions to t_2 and e orbitals have been estimated using c_3^2 and $(c_1^2 + c_2^2)$ from Xα calculations (see text).

allowed $^3T_1{}^a$ parent excited state will contain ~84% of the predicted strong field intensity. The remaining ~16% is predicted to be redistributed to ~1.66 eV higher energy (for the transition to the formally forbidden $^3T_1{}^b$ excited state).

There are three allowed excited state parents in T_d Fe^{II}, only one of which ($^4T_1$) experiences higher state mixing. The allowed parent state is denoted $^4T_1{}^a$, and the higher lying forbidden excited state is $^4T_1{}^b$. Evaluation of the Tanabe−Sugano matrices indicates that the majority (~71%) of the intensity predicted for the $^4T_1{}^a$ parent final state (see Table 6) is actually redistributed to ~1.19 eV higher energy (relative to the allowed $^4T_1{}^a$ state). To define the distribution of intensity for all T_d Fe^{II} pre-edge transitions, the ratios between the dipole strengths of each transition can be employed (see Table 6). These ratios (given in Table 7), combined with the coefficients of excited state mixing, can be used to calculate the pre-edge transition intensity ratios. For transitions to the excited state parents $^4T_2$ and $^4T_1{}^a$, the $^4T_2$:$^4T_1{}^a$ intensity ratio is 1:0.29, and the excited states are separated by 0.23 eV. The higher lying (forbidden) $^4T_1{}^b$ state has an intensity of 0.71 relative to $^4T_2$. The relative contribution of the transition to the e-set of Fe^{II} (the $^4A_2$ parent) requires an estimate of the ratio between the π-covalency [c_3^2] in the e-set and the total ($\sigma + \pi = [c_1^2 + c_2^2]$) covalency of the t_2-set. This ratio can be estimated from an Xα calculation of $Fe^{II}Cl_4^{2-}$ (*vide infra*) which indicates that c_3^2:[$c_1^2 + c_2^2$] ~ 0.64:1. The total intensity ratio between transitions to $^4A_2$ and $^4T_2$ is then predicted to be 0.42:1, with an energy splitting of 0.31 eV. These results are summarized in Table 7.

While T_d $Fe^{III}Cl_4^-$ has no intermediate-strength ligand field mixing, the transition intensity ratio between transitions to the e- and t_2-sets (^5E and $^5T_2$ parents, respectively) can be similarly determined. The ratio between the e-set π-covalency [c_3^2] and the t_2-set covalency [$c_1^2 + c_2^2$] is determined from an Xα calculation (*vide infra*) to be c_3^2:[$c_1^2 + c_2^2$] ~ 0.86:1. The combination of this ratio and the intensity ratios predicted by the dipole strength expressions (Table 6) give the pre-edge transition intensity ratio for $Fe^{III}Cl_4^-$ to be ^5E:$^5T_2$ ~ 0.58:1. The energy splitting between these two parent states is equal to the excited state $10Dq$ and is determined to be 0.49 eV.

D. Determination of Total Experimental Pre-edge Intensity and Calculation of Covalency. On the basis of the intensity ratios and energy splittings derived in the previous section (see Table 7), each pre-edge feature has been broken down into its contributing transitions. Figure 4 shows the experimental data with the contributing pre-edge transitions and their assignments. The transitions were constrained to have the appropriate theoretical intensity ratios and energy splittings.

The strong field dipole strength expressions derived above and given in Table 6 describe the *total* multiplet intensity. For $CuCl_4^{2-}$ (Figure 4a) and $NiCl_4^{2-}$ (Figure 4b) a single transition contributes to the pre-edge, and the total multiplet intensity is that observed in the Results section (Table 2). For $CoCl_4^{2-}$ (Figure 4c), the intensity under the pre-edge feature is *not* the total multiplet intensity. Rather, the total intensity includes the contribution which has been redistributed to higher energy due to mixing in an intermediate-strength ligand field. Thus, the pre-edge feature reflects ~84% of the total (see Table 7), and the total experimental estimate of intensity is obtained by multiplying the observed pre-edge intensity by $^1/_{0.84}$.

The two transitions which contribute to the pre-edge feature in $Fe^{III}Cl_4^-$ are unresolved, but the pre-edge feature is broadened[36] (Figure 4e). The intensities of the two transitions (with fixed energy splittings and intensity ratios) were modeled with a number of different rising edge backgrounds. In each case the sum of the intensities of the two transitions was within the error reported for the intensity of the feature obtained from a one-function fit which was reported in the Results section (Table 2).

For $Fe^{II}Cl_4^{2-}$ (Figure 4d), the observed pre-edge intensity is the sum of transitions to the $^4A_2$, $^4T_2$, and $^4T_1$ parents. The total multiplet intensity must also include the contribution which has been redistributed to higher energy ($^4T_1{}^b$) due to mixing in an intermediate-strength ligand field. The sum of the $^4A_2$, $^4T_2$, and $^4T_1{}^a$ transitions (*i.e.*, the pre-edge peak intensity), compared to the intensity redistributed to the higher lying $^5E \rightarrow {}^4T_1{}^b$ transition, gives a theoretical ratio of 1:0.415. The observed pre-edge feature intensity, then, reflects only 70.7% of the total multiplet intensity. As for $Fe^{III}Cl_4^-$, the sum of the intensities from the transitions which contribute to the pre-edge feature is adequately described by the intensity of the pre-edge feature obtained from a one-function fit (Table 2). Thus, the total multiplet intensity is determined by multiplying the observed pre-edge intensity (Table 2) by $^1/_{0.707}$. Note that this factor rescales only the pre-edge feature intensity. The tail of the $^5E \rightarrow {}^4T_1{}^b$ transition, which contributes intensity in the pre-edge region, is not included because the fitting procedure described in part D of the Experimental Section eliminates its contribution. The total multiplet intensity (the sum of all contributing transitions) for each complex is given in Table 8.

---

(36) Support for the pre-edge assignment in $Fe^{III}Cl_4^-$ is given by the fwhm's required to fit the data. The fwhm of a pre-edge transition is dependent on the resolution of the experiment and on the core-hole lifetime of the Cl 1s hole, both of which should be relatively constant across this series. In each of the $M^{II}Cl_4^{2-}$ spectra the fwhm required to fit the data ranged between 1.04 and 1.18 eV, while the fwhm required to fit the $Fe^{III}Cl_4^-$ was 1.32−1.44 eV. When one function was replaced with two (with the appropriate intensity ratios and energy splitting fixed) in $Fe^{III}Cl_4^-$ (Figure 4e), the fwhm of each of the two transitions which reproduced the data in the pre-edge region ranged between 1.12 and 1.22 eV, in better agreement with the fwhm of the rest of the series.

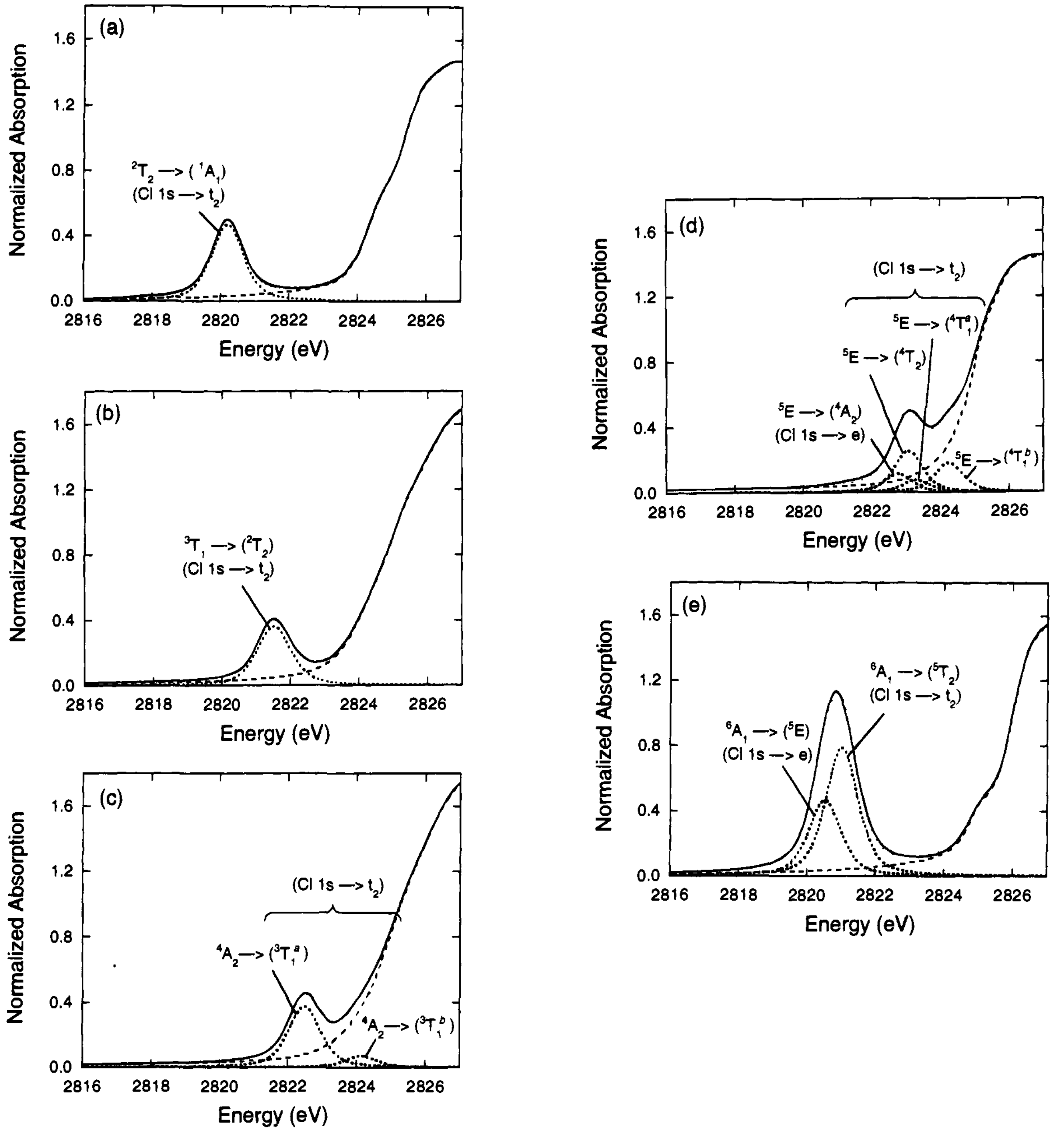

Figure 4. Pre-edge transition assignments for (a) $CuCl_4^{2-}$, (b) $NiCl_4^{2-}$, (c) $CoCl_4^{2-}$, (d) $Fe^{II}Cl_4^{2-}$, and (e) $Fe^{III}Cl_4^{-}$. Transitions are fixed to theoretical intensity ratios and energy splittings (Table 7) and are designated by the ground state of each system and the parent d^{n+1} metal excited state to which the transition occurs. States designated with a "*b*" denote excited states which derive transition intensity from intermediate-strength ligand field mixing.

Table 8. Covalency Analysis of Pre-edge Intensities in MCl_4^{n-} Cl K-Edges

complex	observed pre-edge intensity	factor for intensity distributed to higher energy	total multiplet intensity	covalency reflected in dipole strength (%)
$CuCl_4^{2-}$	0.526 ± 0.017		0.526 ± 0.017	$c_1^2 + c_2^2 = 30.0$
$NiCl_4^{2-}$	0.428 ± 0.018		0.428 ± 0.018	$c_1^2 + c_2^2 = 11.8 \pm 0.6$
$CoCl_4^{2-}$	0.419 ± 0.021	$^1/_{0.84}$	0.497 ± 0.025	$c_1^2 + c_2^2 = 9.0 \pm 0.5$
$Fe^{II}Cl_4^{2-}$	0.427 ± 0.039	$^1/_{0.707}$	0.662 ± 0.061	$c_1^2 + c_2^2 + (^1/_3)c_3^2 = 11.9 \pm 1.2$
$Fe^{III}Cl_4^{-}$	1.505 ± 0.064		1.505 ± 0.064	$c_1^2 + c_2^2 + (^2/_3)c_3^2 = 29.8 \pm 1.6$

The dipole strength expressions in Table 6 can now be applied to the total multiplet intensity to obtain a quantitative estimate of the covalency in each system. Dipole strength is usually equated with absolute, rather than normalized, intensity. To verify that the dipole strength can be applied directly to the data normalized to the edge jump intensity, the dipole strength has been calculated for the edge jump, modeled as a Cl 1s → 4p transition. The dipole strength was determined to be the same for each molecule.[37] Since each normalized edge jump has an intensity of 1.0, the pre-edge intensity dipole strength expressions (Table 6) can reliably be applied to the normalized data.

The coefficients for the ground state wavefunction of D_{4h}

---

[37] The Cl 1s → 4p dipole strength for each case, in terms of one-electron reduced matrix elements, is $D_o = (^2/_3)[\langle a_1||t_2||t_2\rangle^2 + \langle t_2||t_2||a_1\rangle^2 + \langle t_2||t_2||t_2\rangle^2]$.

$CuCl_4^{2-}$ have been determined experimentally from a variety of spectral methods, including EPR superhyperfine analysis. The Cl contribution to the HOMO in D_{2d} $CuCl_4^{2-}$ has been determined experimentally relative to the value of D_{4h} $CuCl_4^{2-}$ and corresponds to ~30% Cl 3p character.[7,38] The value of the Cl 1s → 3p transition intensity ($\langle s|\mathbf{r}|p\rangle^2$) can be estimated by equating the dipole strength expression for $CuCl_4^{2-}$ in Table 6 to the total pre-edge intensity of the complex in Figure 1b and letting the total ($\sigma + \pi$) chloride character be 30% ($[c_1^2 + c_2^2] = 0.30$). This value of $\langle s|\mathbf{r}|p\rangle^2$ can be substituted into the dipole strength expressions for the remaining complexes, and the covalency of each can be obtained from the pre-edge intensity. Note that the uncertainty in the value of $\langle s|\mathbf{r}|p\rangle^2$ derived from the uncertainty in the experimental intensity for $CuCl_4^{2-}$ has been carried through the calculations of covalency for the other complexes. Because the transitions to the parent excited states in $Fe^{II}Cl_4^{2-}$ and $Fe^{III}Cl_4^-$ are not experimentally resolved, the total pre-edge intensity must be equated with the sum of the dipole strength for all contributing transitions (Table 6). For $Fe^{II}Cl_4^{2-}$, $D_0(\text{total}) = (c_1^2 + c_2^2 + (^1/_3)c_3^2)R^2\langle s|\mathbf{r}|p\rangle^2$ and for $Fe^{III}Cl_4^-$, $D_0(\text{total}) = (c_1^2 + c_2^2 + (^2/_3)c_3^2)R^2\langle s|\mathbf{r}|p\rangle^2$.

The Cl $\pi + \sigma$ covalency $[c_1^2 + c_2^2]$ in the t_2-set in $NiCl_4^{2-}$ and $CoCl_4^{2-}$ is calculated to be (11.8 ± 0.6)% and (9.0 ± 0.5)%, respectively, indicating a reduction in covalency relative to $CuCl_4^{2-}$. For $Fe^{II}Cl_4^{2-}$, the covalency derived from the pre-edge intensity is the total Cl 3p character ($\pi + \sigma$) in the t_2-set plus one-third of the 3p character (π) in the e-set $[c_1^2 + c_2^2 + (^1/_3)c_3^2]$ and is determined to be (11.9 ± 1.2)%. The covalency determined for $Fe^{III}Cl_4^-$ is (29.8 ± 1.6)% which corresponds to the total Cl 3p character ($\pi + \sigma$) in the t_2-set plus two-thirds of the 3p character (π) in the e-set $[c_1^2 + c_2^2 + (^2/_3)c_3^2]$. These results are summarized in Table 8.

In the calculation of covalency no approximations in the determination of pre-edge intensity have been made for either $NiCl_4^{2-}$ or $Fe^{III}Cl_4^-$. For $CoCl_4^{2-}$ and $Fe^{II}Cl_4^{2-}$, the total multiplet intensity depends on the excited state values of *Dq* and *B*, and for $Fe^{II}Cl_4^{2-}$, on the relative covalency between the t_2 and e orbital sets from Xα calculations. The error limits given in Table 8 depend only on the uncertainties which derive from the normalization and fitting procedures used in the determination of experimental intensities.

In this analysis the value of the Cl 1s → 3p transition intensity ($\langle s|\mathbf{r}|p\rangle^2$) has been assumed to be constant over the MCl_4^{n-} complexes. In fact, this intensity should be somewhat dependent on the charge on the chloride. As was shown in Analysis, section I (Table 3), the charge on the chloride varies in these complexes by as much as one-third of a charge unit. To ascertain the relationship between the Cl 1s → 3p transition intensity and the Cl charge, the relative oscillator strength of the transitions has been estimated using hydrogenic wavefunctions. The result is dependent on the effective charge (Z_{eff}) in both the Cl 1s and Cl 3p orbitals. The proportionality relationship is given in eq 5.

$$\langle s|\mathbf{r}|p\rangle^2 \; \alpha \frac{(Z_{eff}(s))^{3/2}(Z_{eff}(p))^{5/2}(Z_{eff}(p) + 2Z_{eff}(s))}{(Z_{eff}(p) + Z_{eff}(s))^6} \qquad (5)$$

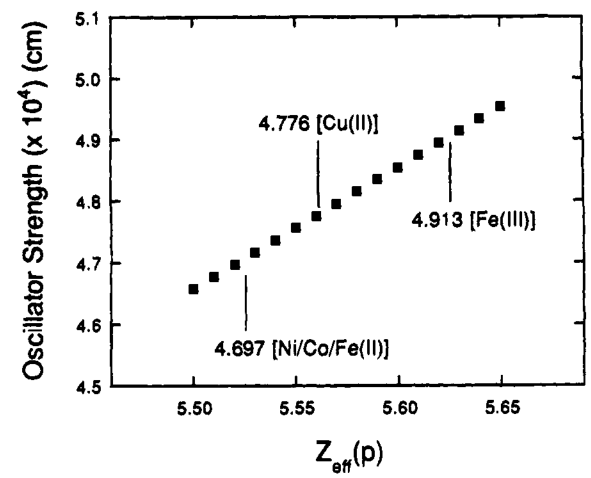

Figure 5. The oscillator strength of the Cl 1s → 3p transition intensity vs $Z_{eff}(p)$, the effective charge of the Cl 3p orbital. In this range of $Z_{eff}(p)$, the relationship is nearly linear. The value of $Z_{eff}(s)$, the effective charge of the Cl 1s orbital, is fixed at 16.7 as calculated by Slater's rules. The $Z_{eff}(p)$ are calculated from Slater's rules and the experimentally determined charge (Table 3). The oscillator strength is 4.697 for Cl bound to Ni, Co, and Fe^{II}, 4.776 for Cl in $Cu^{II}Cl_4^{2-}$ and 4.913 ($\times 10^4$ cm) for Cl in $Fe^{III}Cl_4^-$.

The values of $Z_{eff}(s)$ and $Z_{eff}(p)$ can be estimated using Slater's rules[39] and are calculated using the experimentally determined charges (Table 3) to be $Z_{eff}(s) = 16.7$ and $Z_{eff}(p) = 5.56$, 5.52, and 5.63 for Cl bound to Cu^{II}, Ni^{II}, and Fe^{III}, respectively; the $Z_{eff}(p)$ for Cl bound to Co^{II} and Fe^{II} are equal to that of Cl bound to Ni^{II}. Figure 5 shows the relationship between the Cl 1s → 3p oscillator strength and $Z_{eff}(p)$, with $Z_{eff}(s)$ fixed at 16.7. In the range of $Z_{eff}(p)$ for these complexes, the relationship is nearly linear. While there is clearly an increase in Cl 1s → 3p intensity with increasing $Z_{eff}(p)$ due to the 3p orbital contraction, the absolute change is not very large. These results predict that Cl bound to Ni^{II} should be characterized by a $\langle s|\mathbf{r}|p\rangle^2$ value ~2% less intense than that for Cl bound to Cu^{II}. Between $Fe^{II}Cl_4^{2-}$ and $Fe^{III}Cl_4^-$, an increase in Cl 1s → 3p intensity of ~5% is predicted. Since the effect is small, it is reasonable to assume an approximately constant value of $\langle s|\mathbf{r}|p\rangle^2$ in the above analysis.

E. MCl_4^{n-} Xα Calculations: Comparison to Experimental Results. SCF-Xα-SW calculations have been performed on D_{2d} $CuCl_4^{2-}$ and T_d MCl_4^{n-} (M = Ni^{II}, Co^{II}, Fe^{II}, and Fe^{III}) for comparison to the results of the experimental covalency analysis. The results of these calculations are summarized in Table 9. Supplementary Tables S6–S10 detail orbital energies as well as the calculated valence orbital components for these complexes.

The total Cl character in the t_2-set of orbitals varies from 30% in $CuCl_4^{2-}$ to 15% in $Fe^{II}Cl_4^{2-}$; in $Fe^{III}Cl_4^-$ it is 26%. Further, the Cl 3p component of this covalency, which contributes to the electric dipole intensity of Cl K-edge transitions, varies across the series from 95% in $CuCl_4^{2-}$ to 68% in $Fe^{II}Cl_4^{2-}$; for $Fe^{III}Cl_4^-$ the Cl 3p component is 86%. Thus, the Cl 3p character in each t_2-set (corresponding to $[c_1^2 + c_2^2]$ in the above analysis) varies from ~28% in $CuCl_4^{2-}$ to ~10% in $Fe^{II}Cl_4^{2-}$ and is ~22% in $Fe^{III}Cl_4^-$. The results indicate a trend in Cl 3p covalency over the divalent metal series which is correlated with decreasing effective charge on the metal in going from Cu^{II} to Fe^{II}.

The Cl character in the e-set of $Fe^{II}Cl_4^{2-}$ and $Fe^{III}Cl_4^-$ can be similarly examined. The total e-set Cl-character is 10% in $Fe^{II}Cl_4^{2-}$ and 23% in $Fe^{III}Cl_4^-$. Of the total Cl character in the e-set of $Fe^{II}Cl_4^{2-}$, 65% is Cl $3p_\pi$. Thus, the total Cl $3p_\pi$ contribution (corresponding to c_3^2) is found to be ~6%. In $Fe^{III}Cl_4^-$ 84% of the total Cl-character in the e-set is Cl $3p_\pi$. Thus, the total Cl $3p_\pi$ contribution is ~19% (see Table 9). The increase in both t_2 and e covalency in $Fe^{III}Cl_4^-$ relative to

---

(38) Didziulis, S. V.; Cohen, S. L.; Gewirth, A. A.; Solomon, E. I. *J. Am. Chem. Soc.* **1988**, *110*, 250–268.

(39) Karplus, M.; Porter, R. N. *Atoms and Molecules*; W. A. Benjamin: Menlo Park, CA, 1970; p 229.

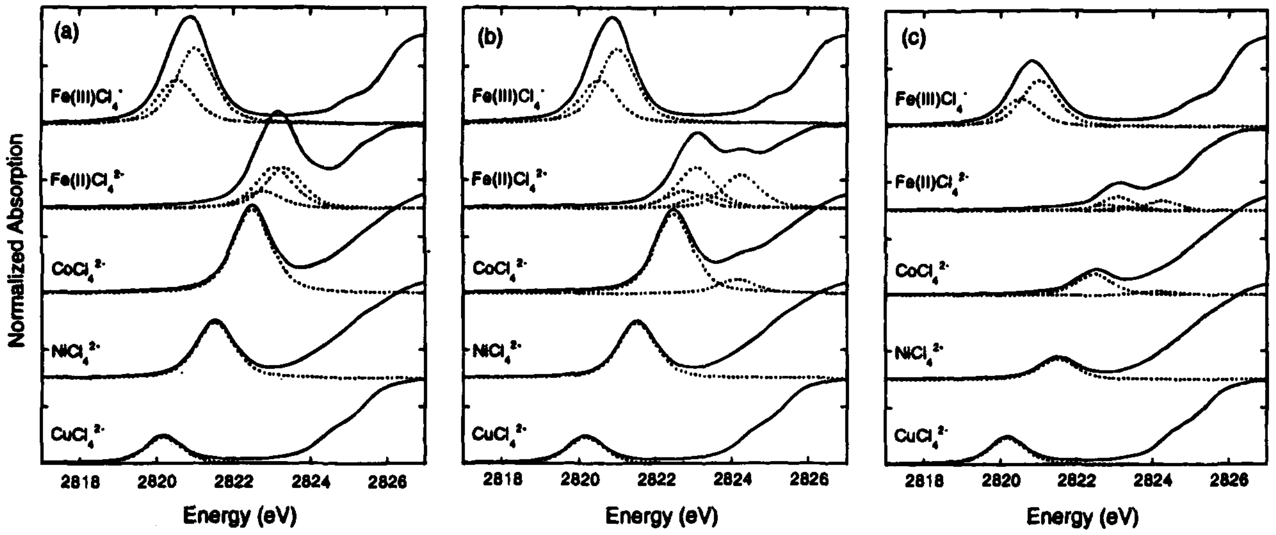

Figure 6. (a) Theoretical Cl K-edge XAS spectra of MCl_4^{n-} complexes with constant t_2-set covalency (30% Cl 3p), e-set covalency fixed with the ratio determined from Xα calculations, and no intermediate ligand field mixing of states. (b) Theoretical Cl K-edge XAS spectra of MCl_4^{n-} complexes with covalencies fixed as in spectrum (a) and intermediate-strength ligand field mixing of states. (c) Experimental Cl K-edge XAS spectra of MCl_4^{n-} complexes. Theoretical spectra in (a) and (b) were generated using experimental transition energies (see Figure 4) and theoretical energy splittings (Table 7). The intensity of each feature was modeled by the fwhm multiplied by the height of the feature. The fwhm for each feature was fixed to that found experimentally for the $CuCl_4^{2-}$ Cl K-edge pre-edge feature. The height was chosen such that the transition intensity, predicted by the dipole strength in each case (for the theoretical covalency 30% Cl 3p), was achieved. The rising edge background used in the theoretical spectra is that used to fit the experimental data for each case. In spectra (a), only transitions to allowed final states are included to simulate the spectra. In spectra (b), transition intensity derived from higher state mixing is included, with the intensity ratios and energy splittings determined in Analysis, section 2 (part C) (see Table 7).

$Fe^{II}Cl_4^{2-}$ is related to the change in oxidation state as well as the concomitant shorter ligand–metal bond length (see Table 1).

In these calculations the remainder of the total Cl character in the t_2- and e-sets (that which is not 3p) is delocalized into diffuse, $l = 2$ orbitals. If the calculations are repeated with $l_{max} = 1$ for the Cl ligands, this $l = 2$ electron density is shifted onto the metal.

For comparison with the experimental covalency analysis, covalencies from the Xα calculations must be correlated to that which is reflected in the multiplet intensity (Table 6): $[c_1^2 + c_2^2]$ for Cu^{II}, Ni^{II}, and Co^{II}; $[c_1^2 + c_2^2 + (^1/_3)c_3^2]$ for Fe^{II}; and $[c_1^2 + c_2^2 + (^2/_3)c_3^2]$ for Fe^{III}. These sums are included in Table 9. The calculated covalency values (Table 9, last column) are within 5% (absolute) of the experimentally determined covalencies (Table 8, last column).

Discussion

Factors Which Determine Pre-edge Intensity. From the analysis of ligand K-edge XAS of a series of first row transition metal MCl_4^{n-} complexes, three factors which contribute to pre-edge transition intensity have been defined: the statistical probability of the occurrence of a pre-edge transition, the degree of excited state mixing in intermediate-strength ligand fields, and the covalency of the metal d-derived orbitals of the site. Each of these contributions is discussed below in greater detail.

Pre-edge intensity is related to the statistical probability of an allowed pre-edge transition. This is reflected in the dipole strength expressions derived for the complexes in these studies. The dipole strength expressions in Table 6 for T_d Cu^{II}, Ni^{II}, and Co^{II} predict an intensity ratio of 1:2:3 (everything else being equal), in proportion to the number of t_2 holes in the ground state of each metal. The dipole strengths of T_d Fe^{II} and Fe^{III} centers follow a similar trend for ground state holes in the t_2- and e-set. Thus, the more orbital vacancies to which spin-allowed transitions are possible, the more intense the pre-edge feature. Figure 6a shows theoretical Cl K-edge spectra for each of the complexes in this study as they would appear in the strong field limit (*e.g.*, no mixing) if the covalency were constant over the series. The covalency of each site is fixed at 0.30 for the t_2-set, with the e-set covalency in $Fe^{II}Cl_4^{2-}$ and $Fe^{III}Cl_4^-$ fixed at the ratios obtained from Xα calculations. The total intensity predicted by the dipole strength is modeled by the fwhm × height, using the same fwhm for all transitions. The pre-edge transition increases by 1:2:3 for Cu^{II}:Ni^{II}:$Co^{II}Cl_4^{2-}$, a result which reflects the statistical probability of the occurrence of a pre-edge transition for each metal complex. The $Fe^{II}Cl_4^{2-}$ pre-edge is somewhat more intense than the $Co^{II}Cl_4^{2-}$ (and $Fe^{III}Cl_4^-$ is more intense than $Fe^{II}Cl_4^{2-}$) due to the additional contributions from transitions to the e-set.

The second contribution to pre-edge feature intensity is mixing between excited states in intermediate-strength ligand fields. This mixing lowers the observed pre-edge intensity by distributing some of the pre-edge intensity to higher energy. Figure 6b shows theoretical Cl K-edge spectra as they would appear for complexes with the same covalency, with the added effect of excited state mixing in intermediate-strength ligand fields. The magnitude of mixing is that determined in Analysis, section II (part C) and the covalency is as above for Figure 6a. The intensity of the pre-edges in $CuCl_4^{2-}$, $NiCl_4^{2-}$, and $Fe^{III}Cl_4^-$ is the same as in Figure 6a, but the intensity of the pre-edges in $CoCl_4^{2-}$ and $Fe^{II}Cl_4^{2-}$ is reduced by ~16 and ~35%, respectively, due to higher state mixing. Note that if the covalency were as high as it is fixed to be in these spectra, the $Fe^{II}Cl_4^{2-}$ spectrum would exhibit a second, higher energy pre-edge feature.

The final contribution to the pre-edge intensity in ligand K-edges comes from the covalency of ligand 3p character in the antibonding metal d-derived orbitals of the complex. The experimental data are shown in Figure 6c (on the same scale as in parts a and b). While the statistical probability of a pre-edge transition increases (Figure 6a), the covalency decreases across the series from Cu^{II} to $Fe^{II}Cl_4^{2-}$. Thus, the total observed pre-edge intensity does not vary significantly across the divalent

Table 9. Summary of SCF-Xα-SW Calculations of MCl_4^{n-} Complexes

T_d complex	total % Cl character in metal d-derived orbitals	3p character as a fraction of total Cl	% Cl 3p character in metal d-derived orbitals	Cl 3p covalency observed in total multiplet intensity (%)
$CuCl_4^{2-}$ (D_{2d})	30	0.95	28.2 ($=c_1^2 + c_2^2$)	28.2
$NiCl_4^{2-}$	19	0.88	16.7 ($=c_1^2 + c_2^2$)	16.7
$CoCl_4^{2-}$	16	0.77	12.3 ($=c_1^2 + c_2^2$)	12.3
$Fe^{II}Cl_4^{2-}$ (t_2)	15	0.68	10.2 ($=c_1^2 + c_2^2$)	12.4 ($=c_1^2 + c_2^2 + (^1/_3)c_3^2$)
(e)	10	0.65	6.5 ($=c_3^2$)	
$Fe^{III}Cl_4^{-}$ (t_2)	26	0.86	22.4 ($=c_1^2 + c_2^2$)	35.3 ($=c_1^2 + c_2^2 + (^2/_3)c_3^2$)
(e)	23	0.84	19.3 ($=c_3^2$)	

series. Further, it is primarily the increase in covalency (augmented by an additional electronic transition to the e-set) between Fe^{III} and Fe^{II} which affects the significant increase in pre-edge intensity observed in the spectrum of $Fe^{III}Cl_4^-$.

Both the statistical probability of the occurrence of a pre-edge transition and the intermediate-strength ligand field excited state mixing can be calculated and their effect on pre-edge intensity determined. Thus, experimental pre-edge intensity, which has had these factors taken into account, provides a direct probe of the ligand 3p character in the antibonding metal d-derived orbitals of a ligand–metal complex.

Covalency in MCl_4^{n-} Complexes. The methodology presented herein allows us to relate ligand XAS pre-edge intensity to metal d-derived orbital covalency in a series of T_d metal–tetrachloride systems. The results are understood in terms of the energetics of bonding. The amount of Cl 3p character in each antibonding orbital in the series is determined by the difference in energy between the metal d orbitals and the Cl 3p orbitals. Covalency will be greatest when the metal d and Cl 3p orbitals are closest in energy. Thus, the variation observed in covalency can be correlated with the effective charge on the metal. For increased effective nuclear charge on the metal, the d orbitals are at deeper binding energy. Analysis of the pre-edge and edge energies of the Cl K-edge spectra shows that the d-manifold energy of the metal centers varies in the order $Cu^{II} < Ni^{II} < Co^{II} < Fe^{II}$ and $Fe^{III} \ll Fe^{II}$.

For complexes with only t_2-vacancies, the t_2-set covalency is greatest in $CuCl_4^{2-}$, which has the deepest d-manifold energy. The t_2-set covalency is least in $Co^{II}Cl_4^{2-}$, which has the highest d-manifold energy. The difference in t_2-set covalency between $CuCl_4^{2-}$ and $NiCl_4^{2-}$ (~30% *vs* ~12%) is larger than the difference between $NiCl_4^{2-}$ and $CoCl_4^{2-}$ (~12% *vs* ~9%). This is consistent with the d-manifold energy differences which are 1.5 eV between $CuCl_4^{2-}$ and $NiCl_4^{2-}$ and only 0.7 eV between $NiCl_4^{2-}$ and $CoCl_4^{2-}$. On the basis of the t_2-set covalency trend in Cu^{II}-, Ni^{II}-, and $Co^{II}Cl_4^{2-}$ and the fact that the Fe^{II} d-manifold is less deep in binding energy than that in Co^{II} by 0.6 eV, it is reasonable to anticipate that the t_2 covalency in $Fe^{II}Cl_4^{2-}$ is somewhat less than that in $Co^{II}Cl_4^{2-}$. This is consistent with the results of Xα calculations (Table 9). The remaining covalency reflected in the pre-edge intensity of $Fe^{II}Cl_4^{2-}$ can be attributed to the additional contribution due to the partially unoccupied e-set.

The difference between the covalencies obtained for $Fe^{III}Cl_4^-$ and $Fe^{II}Cl_4^{2-}$ can also be related to the energetics of bonding. The d-manifold of the Fe^{III} ion is 3.4 eV deeper than that of Fe^{II} due to increased effective nuclear charge and is closer in energy to that of the Cl 3p-orbitals. Both the e- and t_2-set covalency in $Fe^{III}Cl_4^-$ is thus increased relative to $Fe^{II}Cl_4^{2-}$ because of the increased interaction between the metal d and ligand p orbitals.

Summary

Ligand K-edge X-ray absorption spectroscopy has been shown to be a powerful tool in the study of the electronic structure of ligand–metal interactions in open shell metal ions. The technique was developed previously for application to ligand–Cu^{II} covalency[7-9] but has now been extended for application to metal ions with more than one electron (or hole). By use of the expressions derived and the protocol outlined in this study, ligand pre-edge intensity provides a direct probe of the ligand valence p-orbital covalency of a metal–ligand bond. The technique is extended to other d^n systems by application of the analysis presented in this paper.

Ligand K-edges have already been successfully analyzed to quantitate the covalency in the active site electronic structure of blue copper-containing proteins.[8] With the extension of the technique to other d^n metal centers, this work provides the basis for investigations of other metalloproteins and will be of particular importance in the study of bonding in iron–sulfur and related proteins.

Acknowledgment. This research was supported by NSF CHE-9217628 (E.I.S.) and CHE-9121576 (K.O.H.) and by NIH RR-01209 (K.O.H). SSRL operations are funded by the Department of Energy, Office of Basic Energy Sciences. The Biotechnology Program is supported by the National Institutes of Health, Biomedical Research Technology Program, National Center for Research Resources. Further support is provided by the Department of Energy, Office of Health and Environmental Research.

Appendix

In this Appendix is described the application of the irreducible tensor method. This involves the conversion of each pre-edge transition to reduced matrix elements (section I) which are then substituted with matrix elements involving one-electron molecular orbitals (section II). On the basis of these results, the dipole strengths for the transitions to each d^{n+1} parent excited state for each complex are calculated in section III. A description of the analysis in which the symmetry is lowered to D_{2d} for $CuCl_4^{2-}$ is included in section IV.

I. (a) Construction of Reduced Matrix Elements. By use of the irreducible tensor method, each matrix element which may contribute to pre-edge intensity is rewritten, according to Piepho and Schatz,[40] eq 10.2.2 as a $2j$ phase factor and a $3j$ symbol times a many-electron reduced matrix element, $\langle A||\mathbf{r}||B\rangle$, which is independent of the components of the states. This procedure determines which matrix elements are nonzero and will contribute to pre-edge intensity.

Each many-electron reduced matrix element is then further reduced to a one-electron reduced matrix element using eq A1 in which $\langle A||\mathbf{r}||B\rangle$ is rewritten and expanded as

$$\langle \mathcal{A}(a^m(S_1h_1),b^{n-1}(S_2h_2))ShM||\mathbf{r}|| \times$$

$$\mathcal{A}(a^{m-1}(S_1'h_1'),b^n(S_2'h_2'))S'h'M'\rangle = (b,b^{n-1}\,S_2h_2|b^n\,Sh') \times$$

$$\sqrt{n}(|h'||h|)^{1/2}\{h_1h_2h\}\begin{Bmatrix} h' & b & h_2 \\ h_1 & h & \mathrm{T}_2 \end{Bmatrix}\langle a||\mathbf{r}||b\rangle \quad \text{(A1)}$$

where S' is the total spin of the ground state, h' is the many-electron ground state, and M' is the m_s of the ground state. The notation for the excited state is identical, but without the prime designator. The ground state configuration is given as $a^{m-1}b^n$ and the excited state is $a^m b^{n-1}$ (for transitions in terms of holes); a is the ligand core orbital and b is the metal d-derived orbital in each case. S_1' is the total spin and h_1' is the many-electron state arising from the a^{m-1} configuration. $S_2'h_2'$, S_1h_1, S_2h_2 are analogously defined for the b^n, a^m and b^{n-1} configurations, respectively. $|\mathcal{A}(a^{m-1}(S_1'\,h_1'),b^n(S_2'\,h_2'))S'\,h'\,M'\rangle$ denotes the antisymmetrized wavefunction ($\mathcal{A}$) which couples the $S_1'h_1'$ and $S_2'h_2'$ states to make the total $S'h'M'$ ground state. The excited state is similarly defined.

Equation A1 is a modification of Piepho and Schatz[40] eq 20.2.10, which can be simplified for these examples because $m = 1$, $S_1' = 0$, $S' = S$, $h_1' = \mathrm{A}_1$, $a = h_1$, $S_1 = {}^1/_2$, the T_d electric dipole operator $\mathbf{r}$ is t_2, and the coefficient of fractional parentage for the core hole state is always 1. Because these substitutions are applicable to all b^n configurations, eq A1 can be applied to any T_d hole configuration.

Electrons which are in a partially-occupied level which is not involved in a particular transition are called passive electrons. For example, the electrons in the e-set are passive for the following transition written in terms of holes: $\mathrm{a_1^0e^1t_2^3} \rightarrow \mathrm{a_1^1e^1t_2^2}$. For cases with passive electrons ($\mathrm{Fe^{II}}$ and $\mathrm{Fe^{III}}$), an additional step, using Piepho and Schatz,[40] eq 20.3.3, must be taken (before application of eq A1) to decouple the passive electrons from the problem.

(b) Calculation of Reduced Matrix Elements for T_d $\mathrm{MCl_4}^{n-}$. Supplementary Tables S1a–e give the above-described steps in the reduction of the nonzero matrix elements for each pre-edge transition for each T_d $\mathrm{MCl_4}^{n-}$ (M = $\mathrm{Cu^{II}}$, $\mathrm{Ni^{II}}$, $\mathrm{Co^{II}}$, $\mathrm{Fe^{II}}$, and $\mathrm{Fe^{III}}$). Each pre-edge transition is designated by its total excited state (which includes the ligand core hole), by its excited state d^{n+1} parent state (given in parentheses), and by its one-electron orbital transition. The results are given in terms of the squares of each matrix element for summation in the dipole strength expression (eq 2). The necessary $3j$ and $6j$ symbols were obtained from Piepho and Schatz, Tables C.12.1. and C.13.1.[40]

The correlations between allowed excited states and d^{n+1} parent excited states (given in Supplementary Table S1d) for $\mathrm{Fe^{II}Cl_4}^{2-}$ require particular attention. For transitions to the t_2-set in $\mathrm{Fe^{II}Cl_4}^{2-}$ there are two parent excited states, ${}^4\mathrm{T}_1$ and ${}^4\mathrm{T}_2$, constructed from the $\mathrm{et_2^2}$ (d^{n+1}) excited configuration, each of which gives rise to allowed ${}^5\mathrm{T}_1$ and ${}^5\mathrm{T}_2$ final states upon coupling of the ligand a_1 and t_2 holes. The analysis described herein does not trace the ${}^5\mathrm{T}_1$ and ${}^5\mathrm{T}_2$ excited states through these $\mathrm{et_2^2}$ parent states but rather (see Piepho and Schatz[40] eq 20.3.3) requires the states formed from the core holes and t_2-holes ($\mathrm{a_1^1t_2^2}$ and $\mathrm{t_2^1t_2^2}$) be constructed first and then the e-hole to be coupled in. In order to determine which ${}^5\mathrm{T}_1$ and ${}^5\mathrm{T}_2$ final states derive from which $\mathrm{et_2^2}$ (d^{n+1}) parent states, the final state wavefunctions were constructed for both cases according to the method of Piepho and Schatz[40] (eq 19.7.6), and the projection of these ($\mathrm{a_1^1t_2^2}$ or $\mathrm{t_2^1t_2^2}$) states onto the appropriate d^{n+1} parent was determined.

II. Evaluation of Reduced Matrix Elements in Terms of Molecular Orbitals. Evaluation of the one-electron reduced matrix elements, $\langle \mathrm{a_1}||\mathrm{t_2}||\mathrm{t_2}\rangle$, $\langle \mathrm{t_2}||\mathrm{t_2}||\mathrm{t_2}\rangle$, and $\langle \mathrm{t_2}||\mathrm{t_2}||\mathrm{e}\rangle$ requires the evaluation of a single one-electron matrix element $\langle a\alpha|\mathbf{r}|b\beta\rangle$ for each one-electron reduced matrix element. The evaluation of one-electron integrals is described in the Analysis, section IIB, and utilizes eqs 3 and 4. The projections, $p\mathrm{R}$, of eq 4 have been determined for this T_d system using the vectors in Figure 3 and are given in Supplementary Table S2. The result of the evaluation for each nonzero one-electron matrix element $\langle a\alpha|\mathbf{r}|b\beta\rangle$ for the T_d system is given in Supplementary Table S3.

Having obtained the one-electron matrix elements, the values of the one-electron reduced matrix elements ($\langle \mathrm{a_1}||\mathrm{t_2}||\mathrm{t_2}\rangle$, $\langle \mathrm{t_2}||\mathrm{t_2}||\mathrm{t_2}\rangle$, and $\langle \mathrm{t_2}||\mathrm{t_2}||\mathrm{e}\rangle$) can now be determined using Piepho and Schatz,[40] eq 10.2.2 and are given in Supplementary Table S4. Any one of the appropriate one-electron matrix elements in Supplementary Table S3 will yield the same solution for the one-electron reduced matrix element, assuming $\langle \mathrm{s}|\mathbf{r}(x')|\mathrm{p}_{x'}\rangle = \langle \mathrm{s}|\mathbf{r}(y')|\mathrm{p}_{y'}\rangle = \langle \mathrm{s}|\mathbf{r}|\mathrm{p}_{\pi}\rangle$. As seen in Supplementary Table S4, reduced matrix elements involving the t_2-set of orbitals are a sum of $3\mathrm{p}_\sigma(\mathrm{p}_{z'})$- and $3\mathrm{p}_\pi(\mathrm{p}_{x'})$-based integrals, while integrals involving the e-set have only $3\mathrm{p}_\pi(\mathrm{p}_{x'})$-based integrals. Supplementary Table S4 also gives the square of each one-electron reduced matrix element. For transitions to the t_2-set, the square includes cross terms due to the contributions from both σ- and π-based intensity mechanisms.

III. Calculation of Dipole Strength in the Strong Field Limit. The dipole strength (eq 2) is now evaluated for each pre-edge transition by summing the squares of each matrix element contributing to the transition (see Supplementary Table S1, last column). Supplementary Table S5 gives the dipole strength for each pre-edge transition (with its parent excited state designated in parentheses) in terms of one-electron reduced matrix elements. Also given in Supplementary Table S5 are the equivalent dipole strength expressions derived from substitution of the molecular orbital wavefunctions in Supplementary Table S4.

As described in the manuscript, contributions to intensity for transitions which arise from a common d^{n+1} parent state are additive. Further, since the intensity of the pure Cl 1s → 3p transition to the $3\mathrm{p}_{z'}$ orbital is equal in magnitude to those of the $3\mathrm{p}_{x'}$ and $3\mathrm{p}_{y'}$ orbitals, the following substitutions are made, $\langle \mathrm{s}|\mathbf{r}|\mathrm{p}\rangle^2 = \langle \mathrm{s}|\mathbf{r}(z')|\mathrm{p}_{z'}\rangle^2 = \langle \mathrm{s}|\mathbf{r}(x')|\mathrm{p}_{x'}\rangle^2 = \langle \mathrm{s}|\mathbf{r}(y')|\mathrm{p}_{y'}\rangle^2$. The expressions for the total dipole strength for each d^{n+1} parent excited state are given in Table 6. Note that when the dipole strengths for each parent excited state are calculated, the σ-π cross terms cancel. Thus, cross terms do not contribute to observed transition intensity.

IV. Analysis in D_{2d} Symmetry for $\mathrm{CuCl_4}^{2-}$. The $\mathrm{CuCl_4}^{2-}$ geometry is actually D_{2d}. The analysis of pre-edge intensity can be lowered from T_d to D_{2d} using the chain of groups methodology in which the coupling of states of lower symmetry is given by Piepho and Schatz,[40] eq 15.3.3. The integrals in the lower symmetry group are then related to those of the higher symmetry group by Piepho and Schatz,[40] eq 15.4.3.

Lowering the symmetry to D_{2d} results in a splitting of the t_2 HOMO set into b_2 (HOMO) + e-orbitals and the ligand core holes into $\mathrm{a}_1 + \mathrm{b}_2 + \mathrm{e}$. The application to the case of D_{2d} $\mathrm{CuCl_4}^{2-}$ thus involves rewriting the integrals of the T_d analysis as

T_d integrals	D_{2d} integrals chain of groups notation
$\langle \mathrm{A_1}\vert\mathrm{T_2}\vert\mathrm{T_2}\rangle$	$\langle \mathrm{A_1A_1}\vert\mathrm{T_2B_2}\vert\mathrm{T_2B_2}\rangle^{T_d \supset D_{2d}}$*
	$\langle \mathrm{A_1A_1}\vert\mathrm{T_2E}\vert\mathrm{T_2E}\rangle^{T_d \supset D_{2d}}$
$\langle \mathrm{T_2}\vert\mathrm{T_2}\vert\mathrm{T_2}\rangle$	$\langle \mathrm{T_2E}\vert\mathrm{T_2E}\vert\mathrm{T_2B_2}\rangle^{T_d \supset D_{2d}}$*
	$\langle \mathrm{T_2E}\vert\mathrm{T_2B_2}\vert\mathrm{T_2E}\rangle^{T_d \supset D_{2d}}$
	$\langle \mathrm{T_2B_2}\vert\mathrm{T_2E}\vert\mathrm{T_2E}\rangle^{T_d \supset D_{2d}}$

Since the ground state is B_2 for D_{2d} $\mathrm{CuCl_4}^{2-}$, only the first

---

[40] Piepho, S. B.; Schatz, P. N. *Group Theory in Spectroscopy*; Wiley: New York, 1983.

integral in each set (noted with an asterisk [*]) will actually contribute to the dipole strength of a pre-edge transition. Each of these integrals is evaluated using Piepho and Schatz,[40] eq 15.4.3 to obtain the following results:

D_{2d} integral
$\langle A_1A_1\|T_2B_2\|T_2B_2\rangle^{T_d \supset D_{2d}} = \frac{1}{\sqrt{3}}\langle A_1\|\|T_2\|\|T_2\rangle^{T_d}$
$\langle T_2E\|T_2E\|T_2B_2\rangle^{T_d \supset D_{2d}} = \frac{1}{\sqrt{3}}\langle T_2\|\|T_2\|\|T_2\rangle^{T_d}$

The many-electron reduced matrix elements $\langle A_1||T_2||T_2\rangle^{T_d}$ and $\langle T_2||T_2||T_2\rangle^{T_d}$ have been evaluated above in Appendix, section I (Supplementary Table S1a). The dipole strength for D_{2d} $CuCl_4^{2-}$ is thus calculated to be $(^1/_3)R^2(c_1^2+c_2^2)\langle \mathrm{Cl}\ 1s|\mathbf{r}|3p\rangle^2$ which is identical to the result obtained in T_d symmetry.

Xα calculations of the T_d and D_{2d} $CuCl_4^{2-}$ complexes indicate that while the relative σ- and π-covalencies contributions vary, the *total* covalency which is distributed into b_2 and e-sets in D_{2d} is the same as the covalency in the T_d t_2-set. Thus, the analysis herein which calculates $CuCl_4^{2-}$ t_2-covalency using the T_d D_o expression is equivalent to an analysis in D_{2d} which gives the covalency of the b_2 orbital.

Supplementary Material Available: Tables containing the conversion of many-electron integrals to one-electron reduced matrix elements, the T_d axes projections onto Cl p orbitals, the evaluation of one-electron matrix elements, the conversion from reduced matrix elements to matrix elements, the summations for dipole strengths, and the Xα-calculated valence orbitals of MCl_4^{n-} (14 pages). This material is contained in many libraries on microfiche, immediately follows this article in the microfilm version of the journal, can be ordered from the ACS, and can be downloaded from the Internet; see any current masthead page for ordering information and Internet access instructions.

JA942563E